Article

Cell Reports

Wilms Tumor 1b Expression Defines a Pro-regenerative Macrophage Subtype and Is Required for Organ Regeneration in the Zebrafish

Graphical Abstract

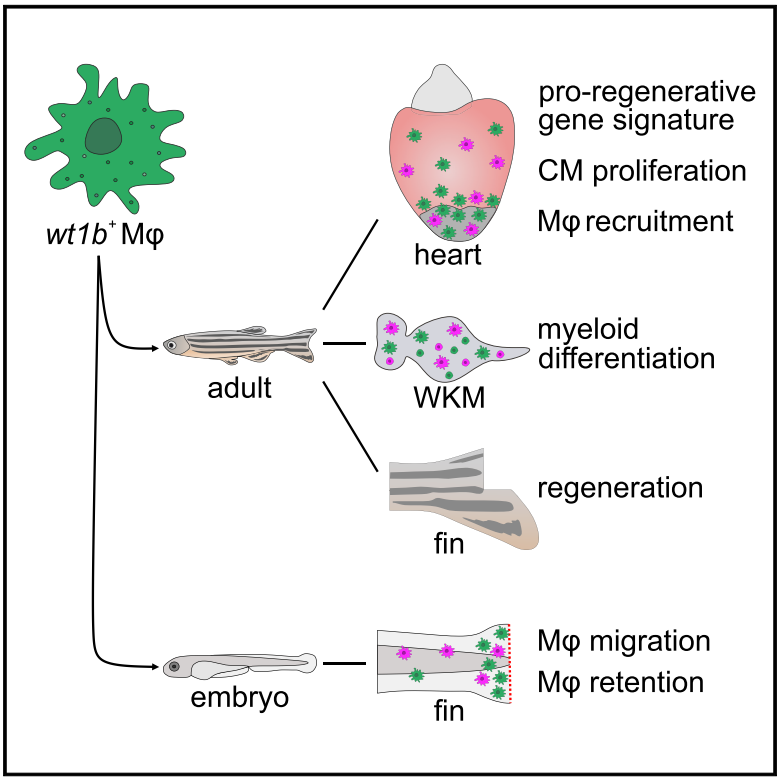

Authors

Andrés Sanz-Morejón, Ana B. García-Redondo, Hanna Reuter, ..., Mercedes Salaices, Christoph Englert, Nadia Mercader

Correspondence

nadia.mercader@ana.unibe.ch

In Brief

Sanz-Morejón et al. identify Wilms tumor 1b (Wt1b)$^{+}$ macrophages with a pro-regenerative gene signature in injured fins and hearts in the zebrafish. They show that Wt1b controls macrophage migration and differentiation. Regeneration is impaired in wt1b mutants, supporting a role for this gene, likely within macrophages, in organ regeneration.

Highlights

- Wt1b^{+} macrophages reveal a pro-regenerative gene expression prolife
- Wt1b controls migration behavior of macrophages during fin and heart regeneration
- Wt1b regulates differentiation of macrophages in the kidney marrow
- *wt1b* mutants reveal impaired fin and heart regeneration

Sanz-Morejón et al., 2019, Cell Reports *28*, 1296–1306
July 30, 2019
https://doi.org/10.1016/j.celrep.2019.06.091

CellPress

OPEN ACCESS
CellPress

Cell Reports
Article

Wilms Tumor 1b Expression Defines a Pro-regenerative Macrophage Subtype and Is Required for Organ Regeneration in the Zebrafish

Andrés Sanz-Morejón,[1,2,7] Ana B. García-Redondo,[2,3,7] Hanna Reuter,[4] Inês J. Marques,[1] Thomas Bates,[4] María Galardi-Castilla,[2] Andreas Große,[4,8] Steffi Manig,[4,8] Xavier Langa,[1] Alexander Ernst,[1] Indre Piragyte,[1] Marius-Alexandru Botos,[1] Juan Manuel González-Rosa,[2,9] Marta Ruiz-Ortega,[5] Ana M. Briones,[3] Mercedes Salaices,[3] Christoph Englert,[4,6] and Nadia Mercader[1,2,10,*]

[1]Institute of Anatomy, University of Bern, 3012 Bern, Switzerland
[2]Centro Nacional de Investigaciones Cardiovasculares (CNIC), 28029 Madrid, Spain
[3]Department of Pharmacology, Universidad Autónoma de Madrid, IIS-Hospital La Paz, Ciber de Enfermedades Cardiovasculares, 28029 Madrid, Spain
[4]Leibniz Institute on Aging–Fritz Lipmann Institute, 07745 Jena, Germany
[5]Cellular Biology in Renal Diseases Laboratory, IIS-Fundación Jiménez Díaz, Universidad Autónoma, 28040 Madrid, Spain
[6]Institute of Biochemistry and Biophysics, Friedrich-Schiller-Universität, 07743 Jena, Germany
[7]These authors contributed equally
[8]Present address: Bio-Rad Medical Diagnostics GmbH, Industriestrasse 1, 63303 Dreieich, Germany
[9]Present address: Cardiovascular Research Center, Massachusetts General Hospital and Harvard Medical School, Boston, MA 02114, USA
[10]Lead Contact
*Correspondence: nadia.mercader@ana.unibe.ch
https://doi.org/10.1016/j.celrep.2019.06.091

SUMMARY

Organ regeneration is preceded by the recruitment of innate immune cells, which play an active role during repair and regrowth. Here, we studied macrophage subtypes during organ regeneration in the zebrafish, an animal model with a high regenerative capacity. We identified a macrophage subpopulation expressing *Wilms tumor 1b* (*wt1b*), which accumulates within regenerating tissues. This *wt1b*$^{+}$ macrophage population exhibited an overall pro-regenerative gene expression profile and different migratory behavior compared to the remainder of the macrophages. Functional studies showed that *wt1b* regulates macrophage migration and retention at the injury area. Furthermore, *wt1b*-null mutant zebrafish presented signs of impaired macrophage differentiation, delayed fin growth upon caudal fin amputation, and reduced cardiomyocyte proliferation following cardiac injury that correlated with altered macrophage recruitment to the regenerating areas. We describe a pro-regenerative macrophage subtype in the zebrafish and a role for *wt1b* in organ regeneration.

INTRODUCTION

Proper control of the inflammatory response, including its duration and the specific immune cell types recruited to the injury site, can determine whether a damaged tissue undergoes fibrotic healing or proceeds to regeneration (Godwin et al., 2017b). In recent years, macrophages have emerged as key players in organ regeneration (Mescher, 2017; Wynn and Vannella, 2016). Macrophage depletion leads to the blockage of several regenerative processes such as limb regeneration in the axolotl (Godwin et al., 2013) and heart regeneration in the zebrafish, axolotl, and neonatal mice (Aurora et al., 2014; Godwin et al., 2017a; Lai et al., 2017).

Macrophages are classically considered to be recruited to the site of damage in two phases (Amici et al., 2017). In the first phase, monocytes are polarized to a pro-inflammatory phenotype by a specific set of cytokines, including tumor necrosis factor (TNF). In the second reparative-regenerative phase, macrophages with different gene signatures are detected at the site of injury (Amici et al., 2017). Whether pro-inflammatory and pro-regenerative phases represent a phenotypic switch within individual macrophages in response to environmental cues or whether newly arriving pro-regenerative macrophage waves displace the original pro-inflammatory population remains unclear. Accumulating evidence challenges the classical M1 and M2 classification and suggests a much more complex spectrum of macrophage polarization states (Murray et al., 2014).

In the zebrafish, a model organism with a high regenerative capacity, macrophages are necessary for the regeneration of the lateral line (Carrillo et al., 2016), fins (Li et al., 2012; Petrie et al., 2014), spinal cord, and the heart (Lai et al., 2017; Tsarouchas et al., 2018). As a first response, macrophages with a pro-inflammatory gene signature are attracted to the site of injury. Similar to that in mammals, the expression of *tnf alpha* (*tnfa*) is a hallmark of zebrafish pro-inflammatory macrophages (Nguyen-Chi et al., 2015). During wound resolution, *tnfa* expression in macrophages is downregulated, suggesting a transition from a pro- to an anti-inflammatory population or polarization state (Nguyen-Chi et al., 2015). Nevertheless, the precise dynamics and changes in the gene expression profile of macrophages during zebrafish organ regeneration remain poorly understood.

In a recent transcriptomics study in mouse hearts, the gene encoding the zinc finger transcription factor Wilms tumor suppressor 1 (Wt1) was found to be expressed in cardiac leukocytes in the neonatal mouse but not in adults, coinciding with the time window during which heart regeneration occurs in mice (Quaife-Ryan et al., 2017). Aberrant *Wt1* expression has been identified in some myeloid leukemias in mammals (Rossi et al., 2016), but *Wt1* has not previously been reported in healthy differentiated myeloid cells. Regarding the heart, *Wt1* has mostly been studied during the formation of the epicardium, the outer layer covering the myocardium (Martínez-Estrada et al., 2010; Moore et al., 1999). Whereas *Wt1* is downregulated in the adult epicardium in the mouse, its expression is reactivated upon myocardial infarction (Zhou et al., 2011). The zebrafish has two *Wt1* orthologs, *wt1a* and *wt1b*, which are expressed in the kidney and mesothelium of several organs, including the heart. Similar to the mouse, *wt1b* is upregulated in the epicardium in response to cardiac damage (González-Rosa et al., 2011; Schnabel et al., 2011) and in sheath cells during notochord repair (Lopez-Baez et al., 2018). Hence, *wt1b* may represent a marker gene for the early phase of regeneration, although its roles during regenerative processes remain unknown.

RESULTS

wt1b Is Expressed in a Subtype of Macrophages

Upon cardiac insult, immune cells are recruited to the injury area and actively participate in debris clearance and inflammatory response control, among other roles. The epicardium, the outer layer covering the myocardium, plays an active role in the recruitment of immune cells to the injured heart (Huang et al., 2012). To characterize macrophage recruitment dynamics following cardiac injury, we crossed the transgenic zebrafish *Tg(wt1b:eGFP)*, which labels epicardium-derived cells (EPDCs) that infiltrate the damaged tissue (Simões and Riley, 2018), with *Tg(mpeg1:mCherry)*, a line widely used to label macrophages in the zebrafish (Ellett et al., 2011).

In double transgenic animals, we performed immunofluorescence staining on heart sections of the cardiac ventricle at different stages post-cryoinjury or sham operated (Figures 1A–1G'''') and co-immunostained with the pan-leukocyte marker L-plastin (Feng et al., 2010). A subset of the *mpeg1*:mCherry$^+$;L-plastin$^+$ population was also positive for *wt1b*:eGFP expression. Flow cytometry analysis further confirmed the presence of *wt1b*:eGFP$^+$;*mpeg1*:mCherry$^+$ cells (Figures 1H and 1I). The percentage of *wt1b:*eGFP$^+$;*mpeg1:*mCherry$^+$ versus *mpeg1*:mCherry$^+$ cells increased at 4 dpi (from 50% ± 16% to 69% ± 11%; the total number of mCherry$^+$ cells was sham 761 ± 347, n = 11; 4 dpi 2,567 ± 1,405, n = 19). At late stages post-injury, 21 dpi, the percentage of *wt1b:eGFP*-expressing macrophages declined (44% ± 10%; total number of mCherry$^+$ cells 1,526 ± 1,342, n = 12).

Histological staining of isolated *wt1b*:eGFP$^+$;*mpeg1*:mCherry$^+$ and *mpeg1*:mCherry$^+$ cells from cryoinjured hearts revealed a typical myeloid cell shape with large cytoplasmic areas and an irregular nuclear shape. Double-positive cells were slightly larger than *mpeg1*:mCherry$^+$ cells (Figures 1J and 1K), suggesting that *wt1b*:eGFP expression distinguished a specific macrophage population in the cryoinjured zebrafish heart. qRT-PCR analysis confirmed that the *wt1b*:eGFP$^+$;*mpeg1*:mCherry$^+$ population expressed higher levels of *wt1b* mRNA than *mpeg1*:mCherry$^+$ cells (Figure 1L), providing evidence that the *Tg(wt1b:eGFP)* reporter line does indeed recapitulate the endogenous *wt1b* expression pattern.

To further test whether *wt1b*:eGFP$^+$;*mpeg1*:mCherry$^+$ cells represent a macrophage population, we confirmed the phagocytic activity of *wt1b*:eGFP$^+$ cells by injecting fluorescently labeled inactivated *Escherichia coli*into the trunk of *Tg(wt1b:eGFP)* larvae followed by *in vivo* imaging (Video S1; observed in 5 of 6 larvae).

Overall, these findings establish the presence of *wt1b*$^+$ macrophages in the heart upon cardiac injury.

wt1b$^+$ Macrophages Present a Pro-regenerative Gene Signature

We next sought to further analyze whether *wt1b* expression reflects the presence of a specific macrophage subtype. To do this, we performed RNA sequencing (RNA-seq) analysis of sorted *wt1b*:eGFP$^+$;*mpeg1*:mCherry$^+$ cells and compared their transcriptome to the rest of *mpeg1*:mCherry$^+$ cells sorted from adult zebrafish hearts at 4 dpi (Figures 2A and S1A–S1C).

In total, 278 genes, including *wt1b* itself, were upregulated in the *wt1b*:eGFP$^+$;*mpeg1*:mCherry$^+$ subset, whereas 314 genes were upregulated in *mpeg1*:mCherry$^+$ cells (Figure 2B; Table S1). The leukocyte marker gene *lcp1*, the myeloid marker genes *spi1a* and *mpeg1.1*, *tnfa* (Nguyen-Chi et al., 2015), and *irf8* (Earley et al., 2018) were not differentially expressed between both populations (Figure 2B; Table S1).

The *wt1b*$^-$ *mpeg1*:mCherry$^+$ population showed the upregulation of genes whose function in macrophages has been associated with pro-inflammatory phenotypes and disease progression such as *tlr7*, *tlr9*, *arg2*, and *rln1* (Table S2). In contrast, the *wt1b*$^+$ macrophages presented an upregulation of genes related to extracellular matrix remodeling and tissue homeostasis restoration such as *timp2b*, *mmp14a*, *vcanb*, *mafba*, *mafbb*, *c1qa*, and *c1qb* genes (Figures 2B, 2C, and S1D; Table S2). In this population, we also detected the upregulation of *il1b*, a cytokine that plays a pivotal role in the modulation of spinal cord regeneration in the zebrafish (Tsarouchas et al., 2018). We also investigated whether direct targets of Wt1, which can act as a transcriptional activator or repressor (Chau and Hastie, 2012), could be found among the differentially expressed genes. *myca*, which is repressed by Wt1, is downregulated, while *mafba and mafbb* genes, which are positively regulated by Wt1, are upregulated in *wt1b*$^+$ macrophages (Dong et al., 2015; Hewitt et al., 1995). This suggests that *wt1b* itself may be involved in the regulation of the pro-regenerative gene signature observed in this population (Figures 2B, 2C, and S1D).

Some of the target and upregulated genes were validated by RNAScope *in situ* hybridization. In this manner, we confirmed the expression of *wt1b*, *mafbb*, and *mmp14a* transcripts in *wt1b*:eGFP$^+$;*mpeg1*:mCherry$^+$ macrophages (Figures S1E–S1J'''').

At the same time, Gene Ontology (GO) biological processes analysis revealed enrichment in blood vessel development, leukocyte migration, and regulation of the inflammatory response, among others, in the *wt1b*$^+$ macrophage population (Figure 2D;

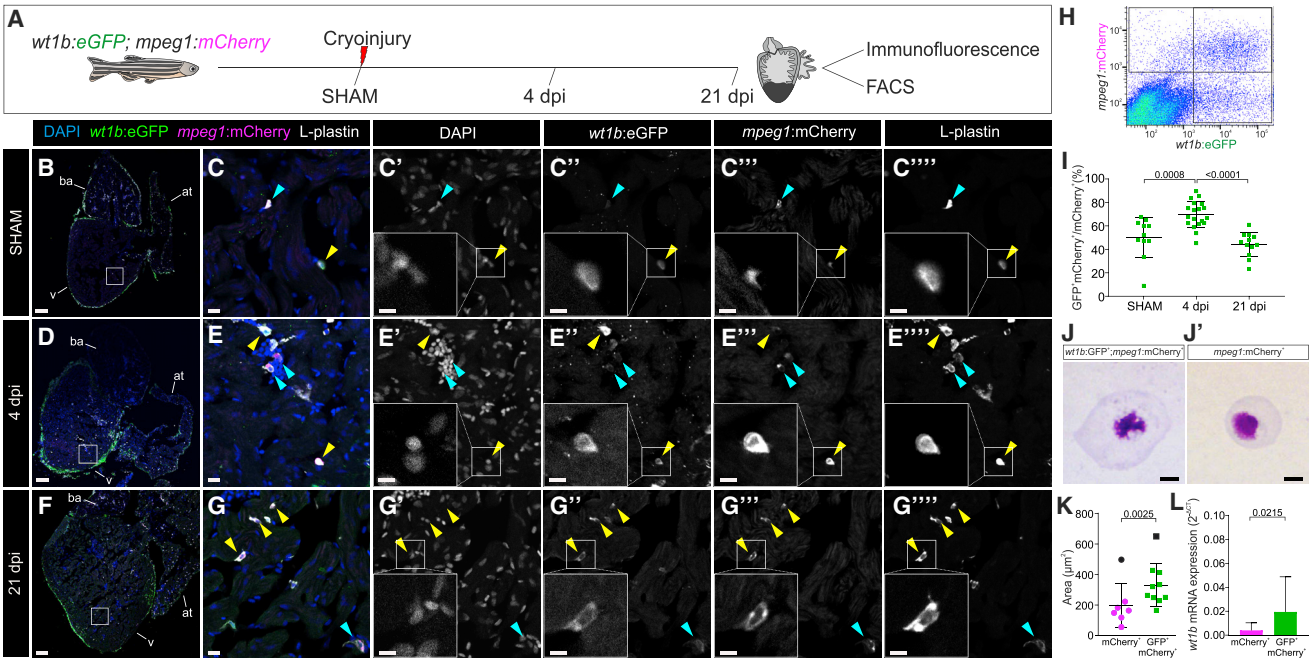

Figure 1. *wt1b*:eGFP Expression Defines a Population of *mpeg1*:mCherry$^+$ Cells in the Zebrafish Heart

(A) *Tg(wt1b:eGFP;mpeg1:mCherry)* adult zebrafish were cryoinjured and hearts were collected to perform FACS or immunofluorescence (IF) staining.

(B–G'''') IF on heart sections. The yellow arrowheads indicate eGFP$^+$;mCherry$^+$;L-plastin$^+$ cells, and the blue arrowheads indicate mCherry$^+$;L-plastin$^+$ cells. (B), (D), and (F) are whole-heart views, remaining panels are zoomed views showing merged (C, E, and G) or single channels. Representative images from sham (n = 7), 4 dpi (n = 14), and 21 dpi (n = 8) processed hearts from 2 experimental replicates are shown.

(H) Representative scatterplot of FACS-sorted cells from *Tg(wt1b:eGFP;mpeg1:mCherry)* hearts at 4 dpi.

(I) Quantification of flow cytometry data showing the percentage of eGFP$^+$;mCherry$^+$/mCherry$^+$ cells at different time points. Statistical significance is calculated by one-way ANOVA, followed by Tukey's multiple comparisons test. Two experimental replicates are shown.

(J and J') May-Grünwald and Giemsa histological staining of mCherry$^+$ and eGFP$^+$;mCherry$^+$ cells isolated from hearts at 4 dpi. Shown are representative examples of 9/10 and 6/8 analyzed cells, for double- and single-positive cells, respectively. Two experimental replicates are shown.

(K) Area measurements of sorted cells from (J) and (J'). Means ± SDs are shown. Calculations were done using Welch's t test. The black points represent statistically significant outliers, by the Grubbs test ($\alpha = 0.05$), excluded from statistical analysis.

(L) qRT-PCR for *wt1b* in mCherry$^+$ and eGFP$^+$;mCherry$^+$ cells isolated from cryoinjured hearts. The points represent biological replicates. Means ± SDs are shown; two-tailed unpaired t test. Ten experimental replicates are shown.

Scale bars, 100 μm (B, D, and F), 10 μm (C, E, G, J, and J'), and 5 μm (magnified views in C'–G'''). at, atrium; ba, bulbus arteriosus; dpi, days post-injury; FACS, fluorescence-activated cell sorting; v, ventricle.

Table S2), further suggesting different cellular behaviors between both populations.

These observations suggest that upon cardiac injury, *wt1b*$^+$ macrophages present a more pro-regenerative gene signature.

wt1b$^+$ Macrophages Preferentially Persist in the Injured Tissue during the Regenerative Phase

The transcriptome analysis suggests different cell behaviors, including migration in *wt1b*$^+$ macrophages. Accordingly, we next examined their migratory capacity and localization at the injury site using a tissue regeneration system that allows *in vivo* monitoring of cell migration—caudal fin resection in zebrafish larvae (Roehl, 2018) (Figure 3A).

In uninjured larvae, *mpeg1*:mCherry$^+$ macrophages within the caudal tail were mostly negative for *wt1b*:eGFP expression (Figures 3B–3C''), whereas *wt1b*:eGFP$^+$; *mpeg1*:mCherry$^+$ cells were present in larval fins post-amputation (Figures 3D–3M''). We analyzed *wt1b*:eGFP expression dynamics during macrophage infiltration and their localization during the regenerative process. During the first 12 h post-amputation (hpa), *mpeg1*:mCherry$^+$ and a few *wt1b*:eGFP$^+$;*mpeg1*:mCherry$^+$ cells reached the site of resection (Figures 3D–3G''; Video S2). This time frame corresponds to a previously described early wave of pro-inflammatory macrophages homing to the site of injury (Nguyen-Chi et al., 2015). Some *mpeg1*:mCherry$^+$ cells that homed to the injury area showed *wt1b*:eGFP upregulation near the amputation site (Video S2), providing evidence for *wt1b* upregulation in a subset of macrophages in response to injury.

At later stages of fin regeneration (between 24 and 72 hpa), when the presence of pro-inflammatory macrophages has been reported to decline (Nguyen-Chi et al., 2015), we observed that *wt1b*:eGFP$^+$;*mpeg1*:mCherry$^+$ cells preferentially accumulated at the regenerating area, whereas *wt1b*$^-$ *mpeg1*:mCherry$^+$ cells were found to be more scattered throughout the larval trunk (Figures 3H–3M''). *In vivo* imaging during 34 hpa revealed that the accumulation of *wt1b*$^+$ macrophages at the regeneration front is mainly a result of the upregulation of *wt1b*:eGFP expression in macrophages during migration rather than the arrival of a

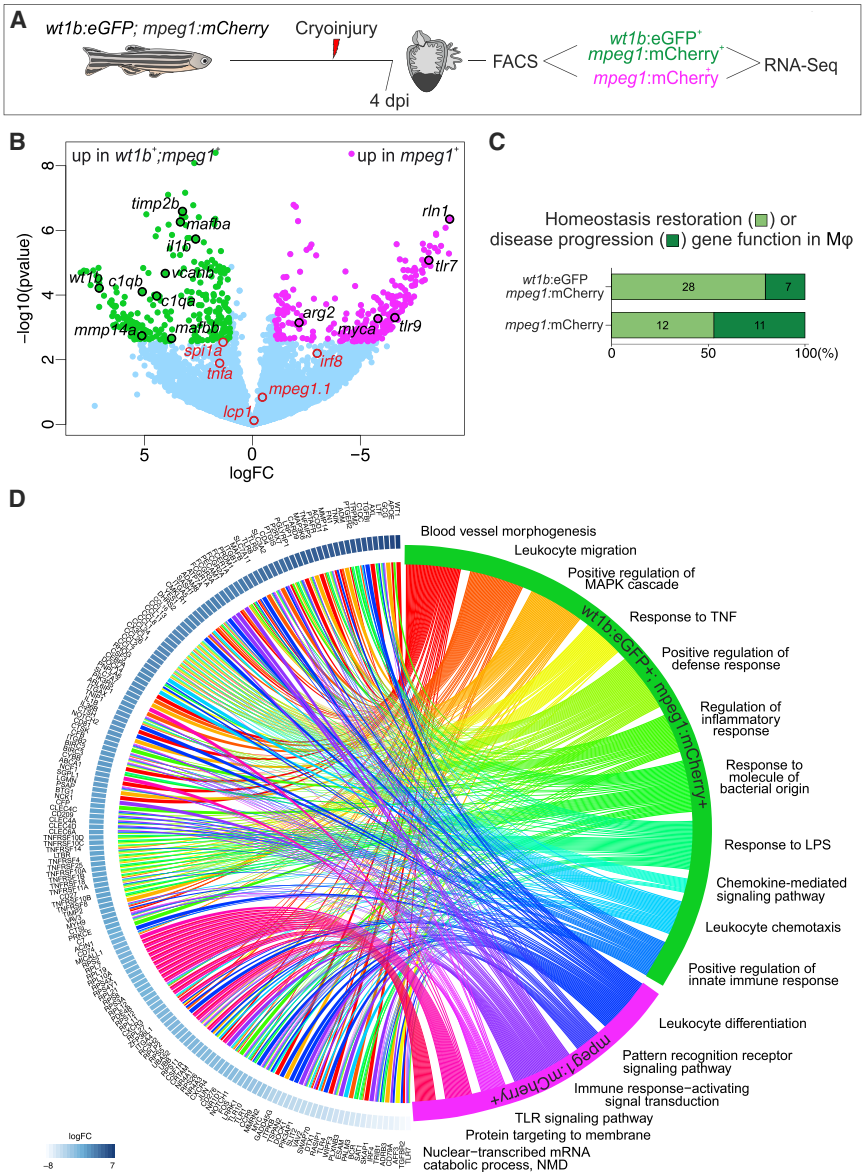

Figure 2. Transcriptome Analysis of *wt1b*:GFP$^+$;*mpeg1*:mCherry$^+$ Cells upon Cardiac Injury

(A) *wt1b*:eGFP$^+$;*mpeg1*:mCherry$^+$ and *mpeg1*:mCherry$^+$ cells were isolated by FACS from adult zebrafish hearts at 4 dpi and their transcriptomes compared by RNA-seq. Biological replicates: 4 each.

(B) Volcano plot. The green and magenta dots correspond to upregulated genes in eGFP;mCherry$^+$ and mCherry$^+$ populations, respectively (adjusted $p < 0.05$, abs($\log_2$FC > 1)). The light blue dots indicate not differentially expressed genes.

(C) Classification of gene function in macrophages according to the literature: light green, genes involved in homeostasis restoration; dark green, genes involved in disease progression. The number of genes considered in each category per population is indicated.

(D) Circular plot of GO biological processes enrichment analysis and their related genes in eGFP$^+$; mCherry$^+$ or mCherry$^+$ cells. The mouse orthologous genes are shown. Differentially expressed genes are linked to their specific pathways. dpi, days post-injury; FACS, fluorescence-activated cell sorting; FC, fold change; Mϕ, macrophage.

See also Figure S1 and Tables S1 and S2.

second wave of *wt1b*:eGFP$^+$ (Video S3; Figure S2). This result suggests a shift of macrophage populations or a polarization state in the regenerating tissue coinciding with the transition from the inflammatory to the regenerative phase, being *wt1b*-expressing macrophages enriched during the latter (Figure 3N).

Wt1b Influences the Migratory Behavior of Macrophages in Response to Injury

We next compared the migration speed of *wt1b*:eGFP$^+$; *mpeg1*:mCherry$^+$ and *mpeg1*:mCherry$^+$ macrophages in the larval caudal fin amputation model. Cell tracking during the first 12 hpa revealed that double-positive cells migrated at a lower speed than *mpeg1*:mCherry$^+$ cells (4.7 ± 2.1 versus 8 ± 0.9 μm/5 min) (Figure 3O).

To investigate the possible role of Wt1b in modulating macrophage migratory behavior upon injury, we generated a *Tg(eGFP-UAS-wt1bDN)* line to inhibit Wt1b function by overexpressing a dominant-negative isoform of *wt1b* (hereafter called *wt1bDN*) in macrophages when crossed with the *Tg(mpeg1:Gal4)* line (Ellett et al., 2011) (Figures S3A–S3D). The wt1bDN truncated protein lacks the four DNA binding zinc finger motifs and has previously been shown to interfere with endogenous WT1 function (Englert et al., 1995; Holmes et al., 1997). As a control, we used a *Tg(eGFP-UAS-RFP;mpeg1:Gal4)* line. *In vivo* imaging of eGFP$^+$ cells was performed in both transgenic lines after amputation of the caudal fin in zebrafish larvae (Figure 3P). We tracked *wt1bDN*-expressing macrophages for 12 hpa of the caudal fin, and mean cell migration speed was compared with that from the control *RFP*-expressing line (Figure 3Q; Video S4). Results showed that the mean migration speed of macrophages overexpressing *wt1bDN* was on average 30% faster than the *RFP*-expressing controls (15 ± 2 versus 11 ± 5 μm/10 min). Consistent with a higher degree of motility, we observed that the number of *wt1bDN*-expressing macrophages persisting in the regenerating caudal fin was reduced compared to the control group at late stages of regeneration (Figures 3R–3T).

Overall, these results show that the endogenous expression of *wt1b* defines a population of macrophages that accumulates after the initial pro-inflammatory response occurring during the early stage of fin regeneration. The finding that *wt1b*$^+$ macrophages remain at the site of injury for a longer period suggests

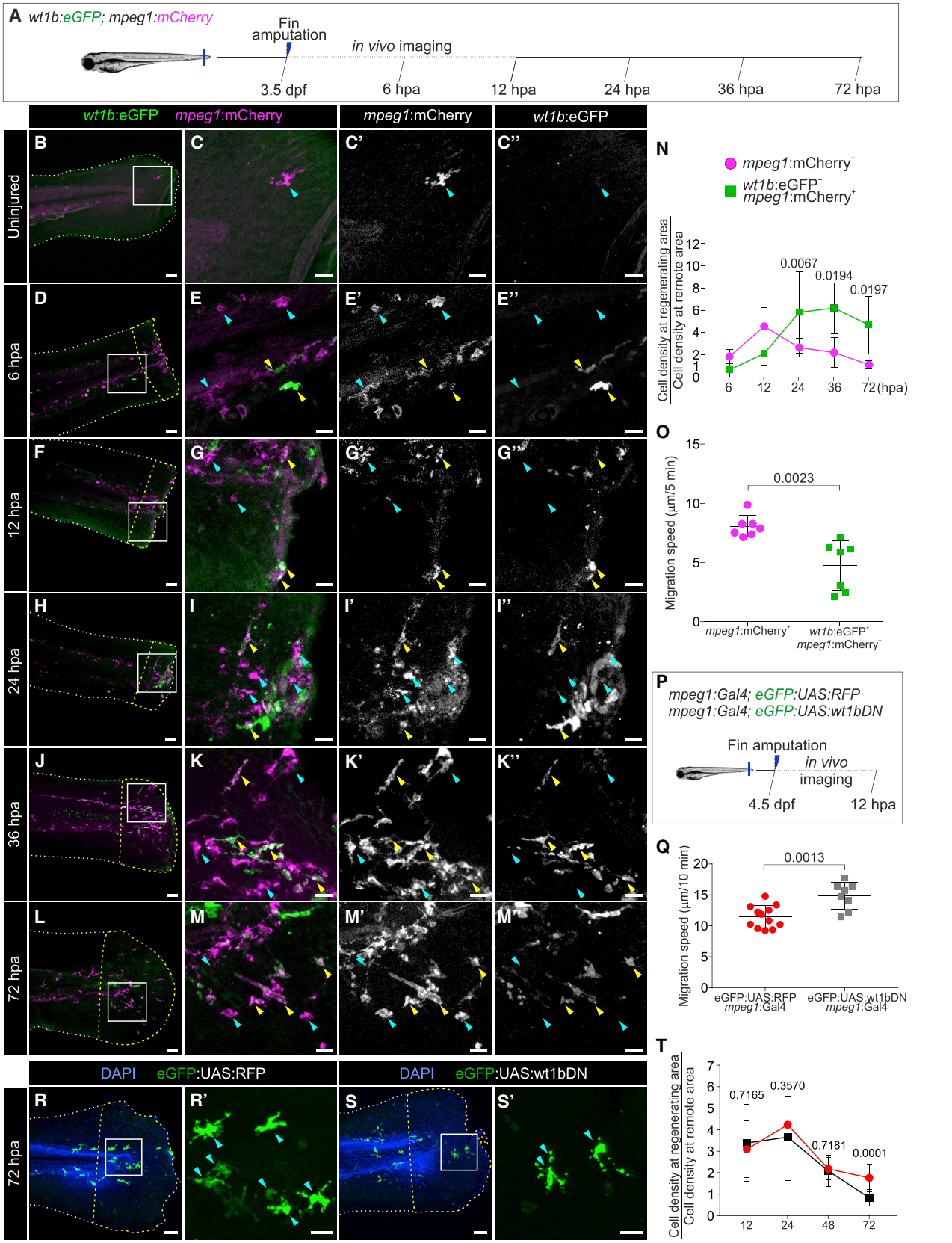

(legend on next page)

that Wt1b plays a role in the retention of macrophages at the regenerating tissue. We demonstrate that Wt1b itself influences macrophage migration dynamics.

Hematopoietic Niche-Derived Cells Can Contribute to the Cardiac *wt1b*$^+$ Macrophage Population

Upon myocardial infarction in the mouse, monocytes derived from the bone marrow and spleen home to the heart and differentiate into macrophages (Honold and Nahrendorf, 2018). The source of macrophages contributing to regeneration in zebrafish remains, nevertheless, unknown.

The kidney marrow is the equivalent of the mammalian bone marrow in the zebrafish. To characterize *wt1b* expression within the hematopoietic niche, we studied the whole kidney marrow (WKM) composition of adult *Tg(wt1b:eGFP;mpeg1:mCherry)* zebrafish by flow cytometry (Figures 4A and 4B). *wt1b*:eGFP$^+$ cells clustered mainly into the hematopoietic progenitor pool (gate 2) (Moore et al., 2016; Traver et al., 2003) (Figures 4B and 4B'). However, as observed in the heart, a subset of *mpeg1*:mCherry$^+$ cells was also *wt1b*:eGFP$^+$ (6.49% ± 4.55%) (Figures 4C and 4D). Histochemical staining of WKM-sorted *wt1b*:eGFP$^+$; *mpeg1*:mCherry$^+$ revealed a typical macrophage morphology and larger cell area than the remainder *mpeg1*:mCherry$^+$ cells (Traver et al., 2003) (Figures 4E and 4F), which is consistent with our observations in the heart (Figures 1J and 1K).

To study whether the *wt1b*$^+$ macrophage subpopulation in the regenerating heart derived from the hematopoietic niche, we transplanted the WKM from adult *Tg(wt1b:eGFP;mpeg1:mCherry)* into irradiated wild types (Figure 4G). After reconstitution of the hematopoietic stem cell niche, the recipients' hearts were cryoinjured and fixed at 4 dpi to assess the presence of *wt1b*-expressing macrophages (Figures 4H–4I''). *wt1b*:eGFP$^+$;*mpeg1*:mCherry$^+$ and *mpeg1*:mCherry$^+$ cells were identified in 5 of 7 animals, suggesting that hematopoietic niche-derived *wt1b*$^+$ macrophages can home to the injured heart.

The Composition of the Hematopoietic Populations Changes in *wt1b* Mutants

Having identified a link between *wt1b* and the immune system, we next investigated its role in the zebrafish adult hematopoietic niche. Given that our *wt1bDN UAS*-driven line is silenced in adults, we used the CRISPR-Cas9 platform to generate a stable mutant *wt1b* line, lacking 5 nucleotides in exon 2 (named *wt1b*$^{\Delta5}$), which is predicted to induce a premature stop codon (Figures S3E and S3F). The loss of *wt1b* expression was confirmed by anti-Wt1 immunostaining in cryoinjured hearts. We failed to detect Wt1 protein in macrophages in *wt1b*$^{\Delta5/\Delta5}$ mutants, but readily observed staining in *wt1b*:eGFP$^+$;*mpeg1*:mCherry$^+$ cells in wild-type hearts (Figures S3G–S3K). In addition, qPCR analysis of embryos revealed a decrease in *wt1b* mRNA expression levels without a concomitant compensatory increase in *wt1a* expression levels (Figure S3L).

We then compared the composition of immune cells in the WKM of *wt1b*$^{+/+}$, *wt1b*$^{+/\Delta5}$, and *wt1b*$^{\Delta5/\Delta5}$ lines (Figures 4J–4J''). Although we observed no changes in lymphoid cells (population 1) or cells from the precursor pool (population 2), in *wt1b*$^{\Delta5/\Delta5}$ animals there was a significant decrease in the numbers of the larger, more granular cells corresponding to myeloid cells, including differentiated macrophages (population 3) (Figure 4J''). Thus, the loss of function of *wt1b* decreases the number of myeloid cells in the adult hematopoietic niche.

Since the genetic background used in this experiment was *Tg(wt1b:eGFP;mpeg1:mCherry)*, we further characterized the eGFP$^+$, mCherry$^+$, and double-positive cells, as well as the non-fluorescent cells in *wt1b*$^{+/+}$, *wt1b*$^{+/\Delta5}$, and *wt1b*$^{\Delta5/\Delta5}$ animals (Figure S4A). We observed no differences in single *wt1b:*eGFP$^+$; *mpeg1:*mCherry$^+$ or double-positive WKM-derived populations (Figure S4B). However, in the non-fluorescent cell population, we detected a significant decrease in the number of myeloid cells (population 3) in *wt1b*$^{\Delta5/\Delta5}$ animals when compared with *wt1b*$^{+/+}$ (Figure S4B). These findings suggest that in the adult kidney

Figure 3. *wt1b*:eGFP$^+$ Macrophages Home to the Site of Injury during Caudal Fin Regeneration, and Wt1b Regulates Their Migratory Behavior

(A) Caudal fins from *Tg(wt1b:eGFP;mpeg1:mCherry)* zebrafish larvae were amputated at 3.5 dpf and either fixed at different time points and processed for IF or embedded for *in vivo* imaging.

(B–M'') Whole-mount IF on caudal fins. Merged and single eGFP and mCherry channels of the magnified views from boxed areas are shown on the right panels. The yellow arrowheads point to double-positive cells, and the blue arrowheads to single mCherry$^+$ cells. The white and yellow dotted lines outline the remote and regenerating areas, respectively. The regenerating area is defined as 100 μm distal from the amputation plane until the fin tip. Maximum intensity projections are shown. Also shown are representative images from 6 hpa (n = 7), 12 hpa (n = 6), 24 hpa (n = 8), 36 hpa (n = 4), and 72 hpa (n = 5) samples from 2 experimental replicates.

(N) Accumulation index of eGFP$^+$;mCherry$^+$ or mCherry$^+$ macrophages at the regenerating area of animals from (D)–(M''). Calculated as cell density at the regenerating area/cell density at the remote area. Two-way ANOVA, followed by Sidak's post hoc test.

(O) Quantification of the migration speed of eGFP$^+$;mCherry$^+$ versus mCherry$^+$ macrophages. The dots indicate mean values for macrophages counted in n = 7 larvae from 3 experimental replicates. Means ± SDs are shown; two-tailed unpaired t test.

(P) Analysis of migratory behavior of macrophages during the first 12 hpa upon Wt1b inhibition by expressing a dominant-negative isoform in macrophages using the Gal4;UAS system.

(Q) Quantification of macrophage migration speed. Means ± SDs are shown. Individual points represent the average migration of all macrophages per embryo from 3 experimental replicates. Two-tailed unpaired Student's t test.

(R–S') Whole-mount IF on caudal fins from *Tg(eGFP:UAS:RFP)* (R) and *Tg(eGFP:UAS:wt1bDN)* (S) lines, both in *Tg(mpeg1:Gal4)* background. (R') and (S') are magnified views of boxed areas in (R) and (S), respectively; arrowheads point to eGFP$^+$ macrophages. The white and yellow dotted lines outline the remote and regenerating areas, respectively. The regenerating area is defined as 100 μm distal from the amputation plane until the fin tip. The maximum intensity projections are shown.

(T) Accumulation index of eGFP:UAS:RFP or eGFP:UAS:wt1bDN macrophages at the regenerating area of animals from (R)–(S') at 12, 24, 48, and 72 hpa, calculated as in (N). An average of n = 12 embryos was analyzed per time point; two-tailed unpaired t test.

Scale bars, 50 μm (B, D, F, H, J, L, R, and S) and 20 μm (magnified views). dpf, days post-fertilization; hpa, hours post-amputation.

See also Figures S2 and S3.

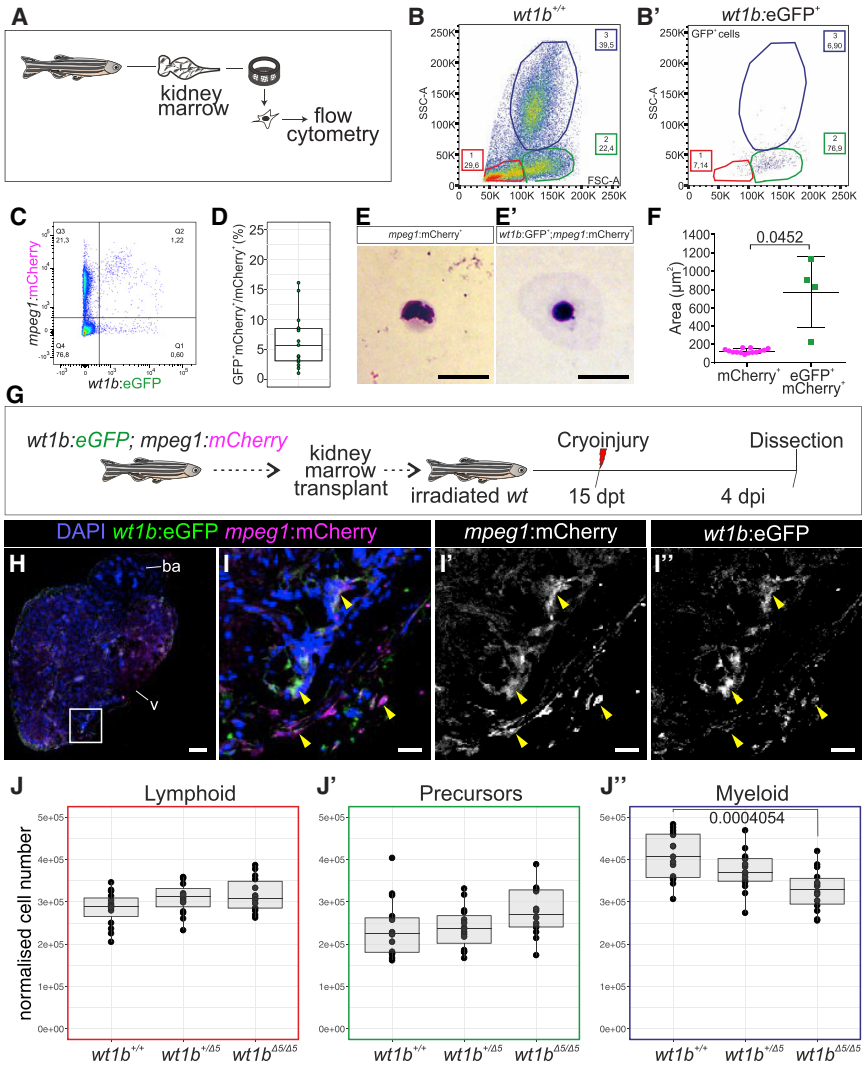

Figure 4. *wt1b*:eGFP$^+$ Cells Are Present in the Hematopoietic Niche and Can Contribute to Cardiac Macrophages in the Regenerating Heart

(A) Whole kidney marrow (WKM) cells from different transgenic or mutant lines were isolated and analyzed by flow cytometry.

(B and B') Forward scatter (FSC-A) versus side scatter (SSC-A) plot of WKM cells. (B) WKM cells of wild-type adult zebrafish gating into 3 distinct populations (gate 1, lymphocytes; gate 2, progenitors; gate 3, myeloid cells). Shown is the percentage of each population normalized to all single alive cells. Erythrocytes were removed from the FACS plot to facilitate data visualization (representative plot of 5 replicates, B, and 2 replicates, B'). (B') eGFP$^+$ cells from the *Tg(wt1b:eGFP)* WKM are enriched in gate 2.

(C) Example plot of FACS purified cells from *Tg(wt1b:eGFP;mpeg1:mCherry)* WKM (representative plot of total n = 15 from 3 experimental replicates).

(D) Quantification of the percentage of eGFP$^+$; mCherry$^+$/mCherry$^+$ WKM cells. Means ± SDs are shown. The points are values from individual animals (n = 15 from 3 experimental replicates)

(E and E') May-Grünwald Giemsa histological staining of mCherry$^+$ and eGFP$^+$;mCherry$^+$ WKM cells. A representative example from a total of 245 mCherry$^+$ and 16 eGFP$^+$;mCherry$^+$ cells (2 independent experiments) is shown.

(F) Cell size measurements of mCherry$^+$ and eGFP$^+$;mCherry$^+$ cells. Means ± SDs are shown. The statistical analysis was performed with Welch's t test.

(G) Tg(*wt1b:eGFP;mpeg1:mCherry*) WKM cells were transplanted into irradiated wild-type hosts. At 15 days post-transplantation (dpt), the host's heart was cryoinjured and fixed at 4 days post-injury (dpi).

(H–I'') IF staining of a heart section from (G).

(I–I'') are merged and single channels of the magnified view of the boxed area in (H). The yellow arrowheads indicate eGFP$^+$;mCherry$^+$ cells. Representative examples from 3 biological replicates from 2 technical replicates are shown.

(J–J'') Composition of immune cells in the WKM of wt1b$^{+/+}$, wt1b$^{+/\Delta5}$, and wt1b$^{\Delta5/\Delta5}$ lines. Boxplots of normalized cell numbers of cell populations in gates 1 (J, lymphoid), 2 (J', precursors), or 3 (J'', myeloid) in wt1b$^{+/+}$ (n = 15), wt1b$^{+/\Delta5}$ (n = 15), and wt1b$^{\Delta5/\Delta5}$ (n = 14) WKM are shown. Data from 3 experimental replicates. Normalized cell numbers relate to cell numbers per 106 events of living single cells. Myeloid cell numbers (J'') are significantly lower in wt1b$^{\Delta5/\Delta5}$ than in wt1b$^{+/+}$ by one-way ANOVA, followed by Tukey's post hoc test.

Scale bars, 20 µm (E, E', and H) and 100 µm (I–I'').

See also Figures S3 and S4.

marrow, Wt1b function is required within a precursor cell population for the maintenance of the myeloid cell pool.

Heart and Fin Regeneration Are Impaired in *wt1b* Mutants

Our findings reveal that *wt1b* expression defines a subset of pro-regenerative macrophages. We next aimed to dissect *wt1b* function during regeneration. To that purpose, we analyzed the regenerative capacity of *wt1b*$^{\Delta5/\Delta5}$ using fin resection and cardiac ventricle cryoinjury. We performed adult caudal fin amputation to *wt1b*$^{\Delta5/\Delta5}$ mutants and *wt1b*$^{+/+}$ wild-type adults, and fin regrowth was quantified periodically until complete regeneration at 18 days post-amputation. We observed a significant delay in fin regrowth from 2 to 5 dpi, showing that fin regeneration is affected in *wt1b*$^{\Delta5/\Delta5}$ mutants (Figures 5A and 5B).

We next studied whether the cardiac regenerative capacity would also be affected in *wt1b* mutants. During cryoinjury, fibrotic tissue deposition is followed by cardiomyocyte proliferation and fibrosis regression (González-Rosa et al., 2011). Ventricular cryoinjury was performed on *wt1b*$^{\Delta5/\Delta5}$ and *wt1b*$^{+/+}$, and cardiomyocyte proliferation was assessed by 5′-bromo-2′-deoxyuridine (BrdU) incorporation at 7 dpi (Figures 5C–5G''). Results showed that cardiomyocyte proliferation in *wt1b*$^{\Delta5/\Delta5}$ mutants was significantly lower than in controls, with a 60% decrease in the number of BrdU$^+$ cardiomyocytes (Figure 5H).

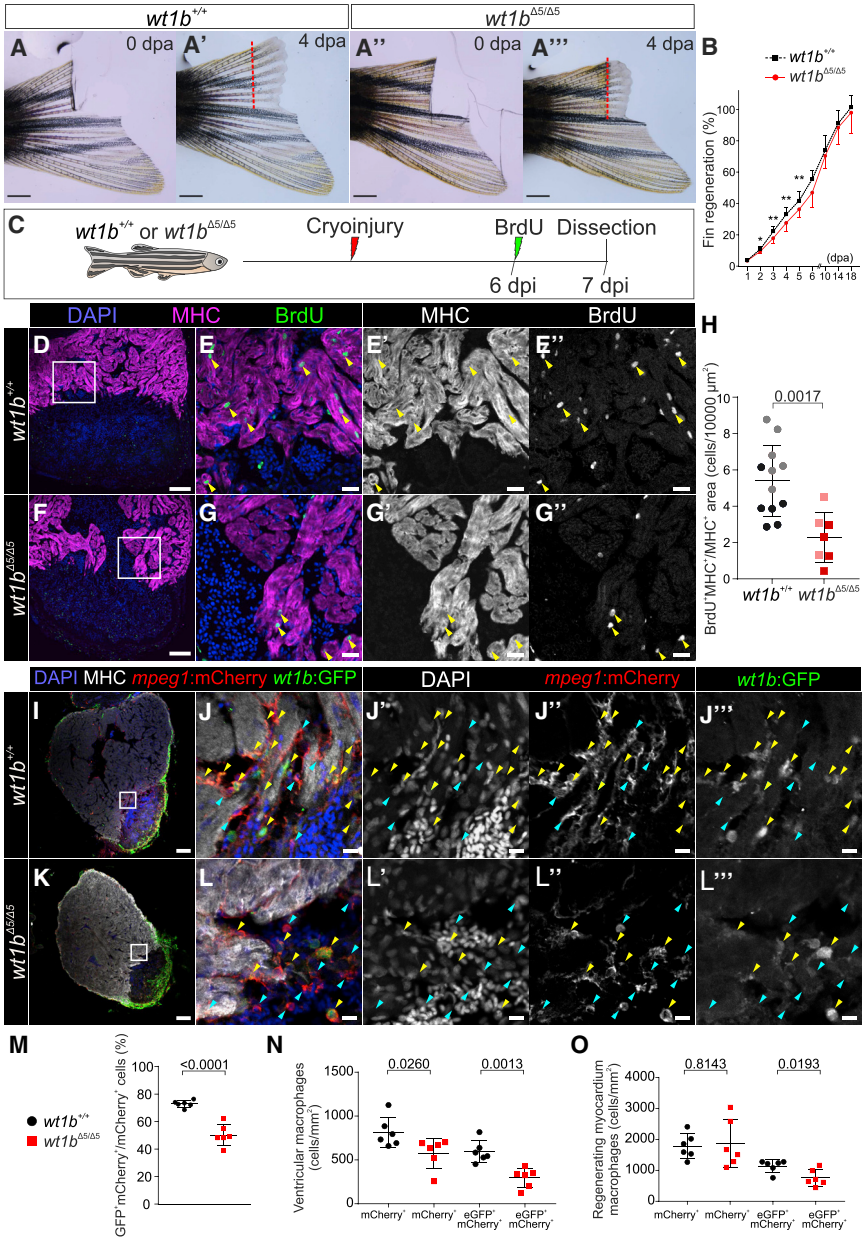

Figure 5. Heart and Fin Regeneration Are Impaired in *wt1b* Mutants

(A–A''') Caudal fin amputation was performed to wild-type *wt1b*$^{+/+}$ and mutant *wt1b*$^{\Delta5/\Delta5}$ adult fish. Fin regrowth was assessed until complete regeneration at 18 dpa. Shown are representative examples at 0 dpa (A and A'') and 4 dpa (A' and A'''). The red dotted line represents the amputation plane.

(B) Quantification of fin regeneration. The 3 most regrown rays were measured per animal and normalized by the initial amputated fin length. The data are from 2 independent experiments: experiment 1 (1–18 dpi), *wt1b*$^{+/+}$ = 7 and *wt1b*$^{\Delta5/\Delta5}$ = 5; experiment 2 (1–6 dpi), *wt1b*$^{+/+}$ = 10 and *wt1b*$^{\Delta5/\Delta5}$ = 10. Means ± SDs are shown; two-tailed unpaired t test (*p < 0.05 and **p < 0.01).

(C) Ventricular cryoinjury was performed on *wt1b*$^{+/+}$ and *wt1b*$^{\Delta5/\Delta5}$ adult fish, and cardiomyocyte proliferation was assessed from 6 to 7 dpi by BrdU incorporation.

(D–G'') IF staining on sections of *wt1b*$^{+/+}$ (D–E'') and *wt1b*$^{\Delta5/\Delta5}$ hearts (F–G''). Nuclei were counterstained with DAPI. (E)–(E'') and (G)–(G'') are merged and single channels of boxed areas in (D) and (F), respectively.

(H) Quantification of cardiomyocyte proliferation. The light- and dark-colored dots represent animals from two independent experiments. Means ± SDs are shown. Two-tailed unpaired Student's t test.

(I–O) Localization of *wt1b*:eGFP;*mpeg1*:mCherry cells in cryoinjured *wt1b*$^{+/+}$ and mutant *wt1b*$^{\Delta5/\Delta5}$ hearts at 7 dpi.

(I–L''') IF staining at 7 dpi heart sections. Nuclei were counterstained with DAPI. Shown are whole heart sections (I and K) and magnified views of merged and single channels (J–J''' and L–L'''). The yellow arrowheads indicate double-positive cells, and the blue arrows indicate *mpeg1*:mCherry^{+} cells.

(M) The percentage of *wt1b*:eGFP^{+};*mpeg1*:mCherry^{+}/*mpeg1*:mCherry^{+} cells per heart section.

(N) Quantification of the number of single- and double-positive cells per area in whole heart sections.

(O) Quantification of the number of single- and double-positive cells in the regenerating myocardium defined as the area of 100 µm adjacent to the injury. In all of the graphs, each dot represents data from one heart section with the maximum injury area. n = 6 hearts analyzed per group from 1 experimental replicate. Means ± SDs are shown; two-tailed unpaired t test.

Scale bars, 1 mm (A–A'''), 100 µm (D, F, I, and K), 20 µm (E–E'' and G–G''), and 10 µm (J–J''' and L–L'''). BrdU, 5′-bromo-2′-deoxyuridine; dpa, days post-amputation; dpi, days post-injury; MHC, myosin heavy chain.

See also Figure S4.

However, neither fibrotic tissue deposition nor fibrosis regression was impaired in *wt1b*$^{\Delta5/\Delta5}$ animals (Figures S4C–S4I).

To test whether the effect on heart regeneration could be a consequence of altered macrophage distribution in *wt1b*$^{\Delta5/\Delta5}$ mutants, we analyzed the composition of *wt1b*:eGFP^{+};*mpeg1*:mCherry^{+} and *mpeg1*:mCherry^{+} cells in hearts from *wt1b*$^{+/+}$ and *wt1b*$^{\Delta5/\Delta5}$ animals at 7 dpi (Figures 5I–5L'''). We found that the percentage of *wt1b*:eGFP^{+};*mpeg1*:mCherry^{+} cells in the heart was reduced in *wt1b*$^{\Delta5/\Delta5}$ compared to *wt1b*$^{+/+}$ (Figure 5M). Furthermore, the number of single- and double-positive cells was also reduced in *wt1b*$^{\Delta5/\Delta5}$ compared to *wt1b*$^{+/+}$ siblings (Figure 5N). Within the 100 µm of myocardium adjacent to the injury area, only the number of *wt1b*:eGFP^{+};*mpeg1*:mCherry^{+} cells was reduced in *wt1b*$^{\Delta5/\Delta5}$, while that of *mpeg1*:mCherry^{+} cells was unaffected (Figure 5O). Thus, the reduction of *wt1b*$^{+}$ macrophages in the regenerating myocardium correlates with the reduced proliferation of cardiomyocytes.

These data support a role for *wt1b* function during adult caudal fin regeneration and cardiomyocyte proliferation upon cardiac injury.

DISCUSSION

Studies exploring the *wt1b* expression pattern during organ regeneration have previously described its upregulation in the epicardium during heart regeneration and in sheath cells during notochord regeneration (González-Rosa et al., 2011; Lopez-Baez et al., 2018; Schnabel et al., 2011). However, a direct role for Wt1 during the regeneration of these structures has not been reported. Our present results demonstrate that *wt1b* upregulation correlates with an injury response in the zebrafish and that Wt1b has a dedicated function during organ regeneration.

We identified a macrophage subtype defined by *wt1b* expression whose genetic profile suggests an overall pro-regenerative behavior, characterized by an anti-inflammatory phenotype and the expression of extracellular matrix remodeling proteins that promote tissue regeneration. The temporal dynamics of *wt1b*$^{+}$ macrophage accumulation during fin regeneration inversely correlate with the dynamics previously observed for *tnfa*$^{+}$ macrophages (Nguyen-Chi et al., 2015, 2017). We found that *tnfa* expression levels at the early stages of the injury response were indistinguishable between *wt1b*$^{+}$ and *wt1b*$^{-}$ cells in the heart. These findings suggest that pro-inflammatory *tnfa*$^{+}$ cells may adopt a reparative character during the later phases of regeneration. The differential expression of some known WT1 targets in *wt1b*$^{+}$ macrophages supports a role for Wt1b as a transcription factor in the definition of this specific macrophage subtype.

The enrichment of *wt1b*$^{+}$ macrophages in the adult heart and larval caudal fin beyond the early phase of the injury response, during which pro-inflammatory macrophages have been described to be predominant, further suggests that *wt1b* expression identifies a population of pro-regenerative macrophages. Following larval caudal fin amputation, we observed both the homing of *wt1b*$^{+}$ macrophages to the site of injury and the upregulation of *wt1b* upon their arrival. This suggests that the homing of different macrophage populations to the damaged tissue coexists with a local change in polarization. We provide evidence that *wt1b* expression defines a subset of macrophages and that Wt1b modulates their migratory behavior.

We also investigated the origin of cardiac *wt1b*$^{+}$ macrophages. Upon myocardial infarction, tissue resident and circulating monocyte-derived macrophages home to the damaged tissue (Chen and Frangogiannis, 2017). Results from transplantation assays suggest that kidney marrow-derived *wt1b*$^{+}$ macrophages can infiltrate into the injured heart. However, the contribution from cardiac resident macrophages in homeostatic conditions cannot be discarded, since circulating macrophages may be reconstituting niches of irradiation-depleted pre-existent cells (Guilliams and Scott, 2017). Furthermore, we show that *wt1b* is required in a cell non-autonomous manner within the hematopoietic niche in the adult zebrafish to maintain the myeloid pool, shedding light on a long-standing debate on the role of *Wt1* in mouse hematopoiesis (Chau and Hastie, 2012).*wt1b* mutants showed decreased maturation of the hematopoietic myeloid lineage, which could influence the number and polarization state of kidney marrow-derived macrophages that home to injured tissues, thus influencing the regenerative process.

Recent studies have highlighted the importance of the immune response and particularly the role of macrophages during regenerative processes (Wynn and Vannella, 2016), including in the fin and the heart (Aurora et al., 2014; Nguyen-Chi et al., 2017). We found delayed adult fin regeneration and impaired cardiomyocyte proliferation upon injury in *wt1b* mutants. Regarding the heart, *wt1b* is not expressed in adult cardiomyocytes. Therefore, the cardiomyocyte proliferation impairment upon injury observed in the *wt1b* mutants must occur in a non-cell-autonomous manner. Impaired cardiomyocyte proliferation correlated with a decrease in *wt1b*$^{+}$ macrophages in the hearts of *wt1b* mutants. Besides the *wt1b*$^{+}$ macrophage subpopulation, *wt1b* is also expressed in EPDCs (González-Rosa et al., 2012). Thus, it cannot be excluded that wt1b also plays a role within the epicardium to support heart regeneration (Wang et al., 2015). Cardiac fibroblasts are derived from EPDCs (Kikuchi et al., 2011) and are the main source of fibrosis in response to cryoinjury (Sánchez-Iranzo et al., 2018). The fact that the fibrotic response is not affected may indicate that Wt1b does not act on regeneration primarily through its role in EPDCs. Our results indicate that Wt1 may play a role in regeneration not only through its function in a specific macrophage population but also through the regulation of myeloid cell differentiation in WKM. Furthermore, the observation that *wt1b* mutants also show delayed fin regeneration upon caudal fin amputation further supports a role for *wt1b* in macrophages during the modulation of the regenerative response.

In conclusion, this study represents the description of a role for *Wt1* during organ regeneration and characterizes a *wt1b*$^{+}$ pro-regenerative macrophage subtype that accumulates within regenerating tissues in the zebrafish. These findings can help to open horizons for the study of macrophage etiology, heterogeneity, and function in a model organism with high regenerative capacity, and they will enrich our understanding of organ regeneration, possibly paving the way for future diagnostic and therapeutic interventions.

STAR★METHODS

Detailed methods are provided in the online version of this paper and include the following:

- KEY RESOURCES TABLE
- LEAD CONTACT AND MATERIALS AVAILABILITY
- EXPERIMENTAL MODEL AND SUBJECT DETAILS
  - Zebrafish
- METHOD DETAILS
  - Construction of mpeg1:mCherry Zebrafish
  - Construction of eGFP:UAS:RFP and eGFP:UAS:wt1bDN Zebrafish
  - Generation of wt1b Mutant (wt1b$^{\Delta5/\Delta5}$) Zebrafish
  - Zebrafish Cardiac Cryoinjuries
  - Zebrafish Caudal Fin Amputations
  - Zebrafish Histological Analysis and Imaging
  - FACS and Flow Cytometry
  - Cytology
  - RT-qPCR on Heart Samples
  - RT-qPCR for wt1a and wt1b in Zebrafish Larvae

- RNaseq Analysis
- GO Biological Processes enrichment analysis
- Macrophage Migration Assay
- Macrophage Intensity Analysis
- Whole Kidney Marrow Transplantation Assays
- Adult Caudal Fin Regeneration upon Amputation
- BrdU Pulse-Chase Experiments during Heart Regeneration
- Macrophage Localization Assessment in Regenerating Hearts
- Quantification of Fibrotic Tissue in Regenerating Hearts

- QUANTIFICATION AND STATISTICAL ANALYSIS
- DATA AND CODE AVAILABILITY

SUPPLEMENTAL INFORMATION

Supplemental Information can be found online at https://doi.org/10.1016/j.celrep.2019.06.091.

ACKNOWLEDGMENTS

We are grateful to the Animal Facility, and the Histology, Microscopy, Cellomics, Genomics, and Bioinformatics Units, in particular, to Manuel Jose Gómez, from Centro Nacional de Investigaciones Cardiovasculares (CNIC) and the Microscopy Imaging Center at the University of Bern (MIC-Bern). We thank Liz Patton for sharing the Wt1 antibody. We thank M.A. Burkhardt for technical support, K. Schubert and M. Locke for assistance with fluorescence-activated cell sorting (FACS) experiments at the Fritz Lipmann Institute (FLI), members of the FLI zebrafish facility and R. Baal for animal husbandry, and D. García-Moreno and V. Mulero for help in cloning the *mpeg1:mCherry* construct. A.B.G.-R. is supported by the Sara Borrell Program (CD11/00165) and CIBER de Enfermedades Cardiovasculares (CB16/11/00286). H.R. was supported by a short-term EMBO fellowship (EMBO STF7204). I.J.M. was supported by a Marie-Sklodowska-Curie postdoctoral fellowship (PIEF-GA-2012-330728). N.M. is supported by Swiss National Science Foundation grant 31003A_15972 and the European Research Council (starting grant 337703–zebra–Heart). The CNIC is supported by the Instituto de Salud Carlos III (ISCIII), the Ministerio de Ciencia, Innovación, y Universidades (MCNU), and the Pro CNIC Foundation and is a Severo Ochoa Center of Excellence (SEV-2015-0505)

AUTHOR CONTRIBUTIONS

A.S.-M. designed and performed most of the experiments. A.B.G.-R. performed most of the preliminary experiments leading to the conclusions of this manuscript. I.J.M. and J.M.G.-R. generated the *Tg(mpeg1:mCherry)* line. A.G. and S.M. generated the *wt1b*$^{\Delta5/\Delta5}$ line. H.R. and T.B. performed some experiments with the *wt1b*$^{\Delta5/\Delta5}$ line. M.B. performed the bioinformatics analysis. I.J.M., M.G.-C., I.P., A.E., J.M.G.-R., and X.L. assisted with the experiments. N.M., C.E., M.R.-O., A.M.B., and M.S. provided funding. A.S.-M. and N.M. wrote the manuscript. A.B.G.-R., I.J.M., H.R., T.B., and C.E. contributed to the interpretation of the results and to writing the manuscript. T.B., H.R., and C.E. conceived the WKM FACS experiments. N.M. conceived the project, designed the experiments, and interpreted the results.

DECLARATION OF INTERESTS

The authors declare no competing interests.

Received: December 19, 2018
Revised: April 25, 2019
Accepted: June 25, 2019
Published: July 30, 2019

REFERENCES

Amici, S.A., Dong, J., and Guerau-de-Arellano, M. (2017). Molecular Mechanisms Modulating the Phenotype of Macrophages and Microglia. Front. Immunol. *8*, 1520.

Aurora, A.B., Porrello, E.R., Tan, W., Mahmoud, A.I., Hill, J.A., Bassel-Duby, R., Sadek, H.A., and Olson, E.N. (2014). Macrophages are required for neonatal heart regeneration. J. Clin. Invest. *124*, 1382–1392.

Carrillo, S.A., Anguita-Salinas, C., Peña, O.A., Morales, R.A., Muñoz-Sánchez, S., Muñoz-Montecinos, C., Paredes-Zúñiga, S., Tapia, K., and Allende, M.L. (2016). Macrophage Recruitment Contributes to Regeneration of Mechanosensory Hair Cells in the Zebrafish Lateral Line. J. Cell. Biochem. *117*, 1880–1889.

Chau, Y.Y., and Hastie, N.D. (2012). The role of Wt1 in regulating mesenchyme in cancer, development, and tissue homeostasis. Trends Genet. *28*, 515–524.

Chen, B., and Frangogiannis, N.G. (2017). Immune cells in repair of the infarcted myocardium. Microcirculation *24*, e12305.

Dong, L., Pietsch, S., Tan, Z., Perner, B., Sierig, R., Kruspe, D., Groth, M., Witzgall, R., Gröne, H.J., Platzer, M., and Englert, C. (2015). Integration of Cistromic and Transcriptomic Analyses Identifies Nphs2, Mafb, and Magi2 as Wilms' Tumor 1 Target Genes in Podocyte Differentiation and Maintenance. J. Am. Soc. Nephrol. *26*, 2118–2128.

Earley, A.M., Graves, C.L., and Shiau, C.E. (2018). Critical Role for a Subset of Intestinal Macrophages in Shaping Gut Microbiota in Adult Zebrafish. Cell Rep. *25*, 424–436.

Ellett, F., Pase, L., Hayman, J.W., Andrianopoulos, A., and Lieschke, G.J. (2011). mpeg1 promoter transgenes direct macrophage-lineage expression in zebrafish. Blood *117*, e49–e56.

Englert, C., Vidal, M., Maheswaran, S., Ge, Y., Ezzell, R.M., Isselbacher, K.J., and Haber, D.A. (1995). Truncated WT1 mutants alter the subnuclear localization of the wild-type protein. Proc. Natl. Acad. Sci. USA *92*, 11960–11964.

Feng, Y., Santoriello, C., Mione, M., Hurlstone, A., and Martin, P. (2010). Live imaging of innate immune cell sensing of transformed cells in zebrafish larvae: parallels between tumor initiation and wound inflammation. PLoS Biol. *8*, e1000562.

Godwin, J.W., Pinto, A.R., and Rosenthal, N.A. (2013). Macrophages are required for adult salamander limb regeneration. Proc. Natl. Acad. Sci. USA *110*, 9415–9420.

Godwin, J.W., Debuque, R., Salimova, E., and Rosenthal, N.A. (2017a). Heart regeneration in the salamander relies on macrophage-mediated control of fibroblast activation and the extracellular landscape. NPJ Regen. Med. *2*, 22.

Godwin, J.W., Pinto, A.R., and Rosenthal, N.A. (2017b). Chasing the recipe for a pro-regenerative immune system. Semin. Cell Dev. Biol. *61*, 71–79.

González-Rosa, J.M., and Mercader, N. (2012). Cryoinjury as a myocardial infarction model for the study of cardiac regeneration in the zebrafish. Nat. Protoc. *7*, 782–788.

González-Rosa, J.M., Martín, V., Peralta, M., Torres, M., and Mercader, N. (2011). Extensive scar formation and regression during heart regeneration after cryoinjury in zebrafish. Development *138*, 1663–1674.

González-Rosa, J.M., Peralta, M., and Mercader, N. (2012). Pan-epicardial lineage tracing reveals that epicardium derived cells give rise to myofibroblasts and perivascular cells during zebrafish heart regeneration. Dev. Biol. *370*, 173–186.

Guilliams, M., and Scott, C.L. (2017). Does niche competition determine the origin of tissue-resident macrophages? Nat. Rev. Immunol. *17*, 451–460.

Hewitt, S.M., Hamada, S., McDonnell, T.J., Rauscher, F.J., 3rd, and Saunders, G.F. (1995). Regulation of the proto-oncogenes bcl-2 and c-myc by the Wilms' tumor suppressor gene WT1. Cancer Res. *55*, 5386–5389.

Holmes, G., Boterashvili, S., English, M., Wainwright, B., Licht, J., and Little, M. (1997). Two N-terminal self-association domains are required for the dominant negative transcriptional activity of WT1 Denys-Drash mutant proteins. Biochem. Biophys. Res. Commun. *233*, 723–728.

Honold, L., and Nahrendorf, M. (2018). Resident and Monocyte-Derived Macrophages in Cardiovascular Disease. Circ. Res. *122*, 113–127.

Huang, G.N., Thatcher, J.E., McAnally, J., Kong, Y., Qi, X., Tan, W., DiMaio, J.M., Amatruda, J.F., Gerard, R.D., Hill, J.A., et al. (2012). C/EBP transcription factors mediate epicardial activation during heart development and injury. Science *338*, 1599–1603.

Kikuchi, K., Gupta, V., Wang, J., Holdway, J.E., Wills, A.A., Fang, Y., and Poss, K.D. (2011). tcf21+ epicardial cells adopt non-myocardial fates during zebrafish heart development and regeneration. Development *138*, 2895–2902.

Kwan, K.M., Fujimoto, E., Grabher, C., Mangum, B.D., Hardy, M.E., Campbell, D.S., Parant, J.M., Yost, H.J., Kanki, J.P., and Chien, C.B. (2007). The Tol2kit: a multisite gateway-based construction kit for Tol2 transposon transgenesis constructs. Dev. Dyn. *236*, 3088–3099.

Lai, S.L., Marín-Juez, R., Moura, P.L., Kuenne, C., Lai, J.K.H., Tsedeke, A.T., Guenther, S., Looso, M., and Stainier, D.Y. (2017). Reciprocal analyses in zebrafish and medaka reveal that harnessing the immune response promotes cardiac regeneration. eLife *6*, e25605.

Li, B., and Dewey, C.N. (2011). RSEM: accurate transcript quantification from RNA-Seq data with or without a reference genome. BMC Bioinformatics *12*, 323.

Li, L., Yan, B., Shi, Y.Q., Zhang, W.Q., and Wen, Z.L. (2012). Live imaging reveals differing roles of macrophages and neutrophils during zebrafish tail fin regeneration. J. Biol. Chem. *287*, 25353–25360.

Li, P., Lahvic, J.L., Binder, V., Pugach, E.K., Riley, E.B., Tamplin, O.J., Panigrahy, D., Bowman, T.V., Barrett, F.G., Heffner, G.C., et al. (2015). Epoxyeicosatrienoic acids enhance embryonic haematopoiesis and adult marrow engraftment. Nature *523*, 468–471.

Lopez-Baez, J.C., Simpson, D.J., LLeras Forero, L., Zeng, Z., Brunsdon, H., Salzano, A., Brombin, A., Wyatt, C., Rybski, W., Huitema, L.F.A., et al. (2018). *Wilms Tumor 1b* defines a wound-specific sheath cell subpopulation associated with notochord repair. eLife *7*, e30657.

Martin, M. (2011). Cutadapt removes adapter sequences from high-throughput sequencing reads. EMBnet J. *17*, 10.

Martínez-Estrada, O.M., Lettice, L.A., Essafi, A., Guadix, J.A., Slight, J., Velecela, V., Hall, E., Reichmann, J., Devenney, P.S., Hohenstein, P., et al. (2010). Wt1 is required for cardiovascular progenitor cell formation through transcriptional control of Snail and E-cadherin. Nat. Genet. *42*, 89–93.

Mescher, A.L. (2017). Macrophages and fibroblasts during inflammation and tissue repair in models of organ regeneration. Regeneration (Oxf.) *4*, 39–53.

Moore, A.W., McInnes, L., Kreidberg, J., Hastie, N.D., and Schedl, A. (1999). YAC complementation shows a requirement for Wt1 in the development of epicardium, adrenal gland and throughout nephrogenesis. Development *126*, 1845–1857.

Moore, J.C., Tang, Q., Yordán, N.T., Moore, F.E., Garcia, E.G., Lobbardi, R., Ramakrishnan, A., Marvin, D.L., Anselmo, A., Sadreyev, R.I., and Langenau, D.M. (2016). Single-cell imaging of normal and malignant cell engraftment into optically clear prkdc-null SCID zebrafish. J. Exp. Med. *213*, 2575–2589.

Murray, P.J., Allen, J.E., Biswas, S.K., Fisher, E.A., Gilroy, D.W., Goerdt, S., Gordon, S., Hamilton, J.A., Ivashkiv, L.B., Lawrence, T., et al. (2014). Macrophage activation and polarization: nomenclature and experimental guidelines. Immunity *41*, 14–20.

Neumann, K., Grittner, U., Piper, S.K., Rex, A., Florez-Vargas, O., Karystianis, G., Schneider, A., Wellwood, I., Siegerink, B., Ioannidis, J.P., et al. (2017). Increasing efficiency of preclinical research by group sequential designs. PLoS Biol. *15*, e2001307.

Nguyen-Chi, M., Laplace-Builhe, B., Travnickova, J., Luz-Crawford, P., Tejedor, G., Phan, Q.T., Duroux-Richard, I., Levraud, J.P., Kissa, K., Lutfalla, G., et al. (2015). Identification of polarized macrophage subsets in zebrafish. eLife *4*, e07288.

Nguyen-Chi, M., Laplace-Builhé, B., Travnickova, J., Luz-Crawford, P., Tejedor, G., Lutfalla, G., Kissa, K., Jorgensen, C., and Djouad, F. (2017). TNF signaling and macrophages govern fin regeneration in zebrafish larvae. Cell Death Dis. *8*, e2979.

Perner, B., Englert, C., and Bollig, F. (2007). The Wilms tumor genes wt1a and wt1b control different steps during formation of the zebrafish pronephros. Dev. Biol. *309*, 87–96.

Petrie, T.A., Strand, N.S., Yang, C.T., Rabinowitz, J.S., and Moon, R.T. (2014). Macrophages modulate adult zebrafish tail fin regeneration. Development *141*, 2581–2591.

Pfaffl, M.W. (2001). A new mathematical model for relative quantification in real-time RT-PCR. Nucleic Acids Res. *29*, e45.

Pfaffl, M.W., Horgan, G.W., and Dempfle, L. (2002). Relative expression software tool (REST) for group-wise comparison and statistical analysis of relative expression results in real-time PCR. Nucleic Acids Res. *30*, e36.

Quaife-Ryan, G.A., Sim, C.B., Ziemann, M., Kaspi, A., Rafehi, H., Ramialison, M., El-Osta, A., Hudson, J.E., and Porrello, E.R. (2017). Multicellular Transcriptional Analysis of Mammalian Heart Regeneration. Circulation *136*, 1123–1139.

Robinson, M.D., McCarthy, D.J., and Smyth, G.K. (2010). edgeR: a Bioconductor package for differential expression analysis of digital gene expression data. Bioinformatics *26*, 139–140.

Roehl, H.H. (2018). Linking wound response and inflammation to regeneration in the zebrafish larval fin. Int. J. Dev. Biol. *62*, 473–477.

Rossi, G., Minervini, M.M., Carella, A.M., Melillo, L., and Cascavilla, N. (2016). Wilms' Tumor Gene (WT1) Expression and Minimal Residual Disease in Acute Myeloid Leukemia. In Wilms Tumor, M.M. van den Heuvel-Eibrink, ed. (Codon Publications).

Sánchez-Iranzo, H., Galardi-Castilla, M., Sanz-Morejón, A., González-Rosa, J.M., Costa, R., Ernst, A., Sainz de Aja, J., Langa, X., and Mercader, N. (2018). Transient fibrosis resolves via fibroblast inactivation in the regenerating zebrafish heart. Proc. Natl. Acad. Sci. USA *115*, 4188–4193.

Schnabel, K., Wu, C.C., Kurth, T., and Weidinger, G. (2011). Regeneration of cryoinjury induced necrotic heart lesions in zebrafish is associated with epicardial activation and cardiomyocyte proliferation. PLoS One *6*, e18503.

Simões, F.C., and Riley, P.R. (2018). The ontogeny, activation and function of the epicardium during heart development and regeneration. Development *145*, dev155994.

Stachura, D.L., Reyes, J.R., Bartunek, P., Paw, B.H., Zon, L.I., and Traver, D. (2009). Zebrafish kidney stromal cell lines support multilineage hematopoiesis. Blood *114*, 279–289.

Traver, D., Paw, B.H., Poss, K.D., Penberthy, W.T., Lin, S., and Zon, L.I. (2003). Transplantation and in vivo imaging of multilineage engraftment in zebrafish bloodless mutants. Nat. Immunol. *4*, 1238–1246.

Tsarouchas, T.M., Wehner, D., Cavone, L., Munir, T., Keatinge, M., Lambertus, M., Underhill, A., Barrett, T., Kassapis, E., Ogryzko, N., et al. (2018). Dynamic control of proinflammatory cytokines Il-1β and Tnf-α by macrophages in zebrafish spinal cord regeneration. Nat. Commun. *9*, 4670.

Villefranc, J.A., Amigo, J., and Lawson, N.D. (2007). Gateway compatible vectors for analysis of gene function in the zebrafish. Dev. Dyn. *236*, 3077–3087.

Walter, W., Sánchez-Cabo, F., and Ricote, M. (2015). GOplot: an R package for visually combining expression data with functional analysis. Bioinformatics *31*, 2912–2914.

Wang, J., Cao, J., Dickson, A.L., and Poss, K.D. (2015). Epicardial regeneration is guided by cardiac outflow tract and Hedgehog signalling. Nature *522*, 226–230.

Wynn, T.A., and Vannella, K.M. (2016). Macrophages in Tissue Repair, Regeneration, and Fibrosis. Immunity *44*, 450–462.

Yu, G., Wang, L.G., Han, Y., and He, Q.Y. (2012). clusterProfiler: an R package for comparing biological themes among gene clusters. OMICS *16*, 284–287.

Zhou, B., Honor, L.B., He, H., Ma, Q., Oh, J.H., Butterfield, C., Lin, R.Z., Melero-Martin, J.M., Dolmatova, E., Duffy, H.S., et al. (2011). Adult mouse epicardium modulates myocardial injury by secreting paracrine factors. J. Clin. Invest. *121*, 1894–1904.

STAR★METHODS

KEY RESOURCES TABLE

REAGENT or RESOURCE	SOURCE	IDENTIFIER
Antibodies		
Chicken polyclonal anti-GFP	Aves Labs	Cat#GFP-1010; RRID:AB_2307313
Mouse living colors polyclonal anti-DsRed	Takara Bio	Cat#632392; RRID:AB_2801258
Rat monoclonal anti-mCherry	Thermo Fisher Scientific	Cat#M11217, RRID:AB_2536611
Mouse monoclonal anti-myosin (for paraffin sections)	Developmental Studies Hybridoma Bank	Cat#MF 20, RRID:AB_2147781
Mouse monoclonal anti-myosin (for gelatin sections)	Developmental Studies Hybridoma Bank	Cat#f59, RRID:AB_528373
Mouse monoclonal anti-BrdU	BD Biosciences	Cat#563445, RRID:AB_2738210
Rabbit anti-L-Plastin	Paul Martin lab	N/A
Rabbit anti-Wt1	Lopez-Baez et al., 2018	N/A
Goat anti-Chicken IgY (H+L) Secondary Antibody, Alexa Fluor 488	Thermo Fisher Scientific	Cat#A-11039, RRID:AB_2534096
Goat anti-Rabbit IgG (H+L) Superclonal Secondary Antibody, Alexa Fluor 647	Thermo Fisher Scientific	Cat#A27040, RRID:AB_2536101
Goat anti-Mouse IgG1 Cross-Adsorbed Secondary Antibody, Alexa Fluor 647	Thermo Fisher Scientific	Cat#A-21240, RRID:AB_2535809
Biotin-SP-AffiniPure F(ab')2 Fragment Goat Anti-Rabbit IgG (H+L) antibody	Jackson ImmunoResearch Labs	Cat#111-066-003, RRID:AB_2337966
Biotin-SP-AffiniPure Goat Anti-Rat IgG (H+L)	Jackson ImmunoResearch Labs	Cat#112-065-167, RRID:AB_2338179
Streptavidin Cy3 conjugate	Thermo Fisher Scientific	Cat#SA1010
Streptavidin Cy5 conjugate	Thermo Fisher Scientific	Cat#SA1011
Chemicals, Peptides, and Recombinant Proteins		
16% Paraformaldehyde (formaldehyde) aqueous solution	Electron Microscopy Sciences	Cat#15710
N-Phenylthiourea (PTU)	Sigma-Aldrich	Cat#P7629
5-Bromo-2′-deoxyuridine (BrdU)	Sigma-Aldrich	Cat#B5002
Phosphate buffered saline (PBS)	Sigma-Aldrich	Cat#P4417
Fetal Bovine Serum (FBS)	Sigma-Aldrich	Cat#F2442
Ethyl 3-aminobenzoate methanesulfonate (Tricaine)	Sigma-Aldrich	Cat#E10521
Trypsin / EDTA	Thermo Fisher Scientific	Cat#15400054
Tri Reagent	Sigma-Aldrich	Cat#T9424
4 ', 6-diamidino-2-phenylindole dihydrochloride (DAPI)	Merck	Cat#124653
Critical Commercial Assays		
Q5 High-Fidelity DNA Polymerase	New England Biolabs	Cat#M0491
Gibson Assembly Master Mix	New England Biolabs	Cat#E2611
Zymoclean Gel DNA Recovery Kit	New England Biolabs	Cat#D4007
DNA Clean & Concentrator	New England Biolabs	Cat#D4013
DreamTaq Green PCR Master Mix	Thermo Fisher Scientific	Cat#K1081
Quick-Stick Ligase	Bioline	Cat#BIO-27027
High-Capacity cDNA Reverse Transcription Kit	Thermo Fisher Scientific	Cat#4368813
QuantiTect Rev. Transcription Kit	QIAGEN	Cat#205310
PicoPure RNA Isolation Kit	Thermo Fisher Scientific	Cat#KIT0204
PowerUp SYBR Green Master Mix	Thermo Fisher Scientific	Cat#A25742
SYBR GreenER	Thermo Fisher Scientific	Cat#11762100
mMESSAGE mMACHINE T7 Transcription Kit	Thermo Fisher Scientific	Cat#AM1344
iScript cDNA synthesis kit	Bio-Rad	Cat#1708890
SYTOX Blue Dead Cell Stain	Thermo Fisher Scientific	Cat#S34857

(*Continued on next page*)

Continued		
REAGENT or RESOURCE	SOURCE	IDENTIFIER
Deposited Data		
Raw bulk RNA-seq wt1b:eGFP+;mpeg1:mCherry+ versus wt1b:eGFP-;mpeg1:mCherry+ cells at 4 days post ventricular cryoinjury	This paper	GEO: GSE115381
Experimental Models: Organisms/Strains		
Zebrafish: *Tg(wt1b:eGFP)*^{li1Tg}	N/A	ZDB-ALT-071127-1
Zebrafish: *Tg(mpeg1:mCherry)*	This paper	N/A
Zebrafish: *Tg(GFP-5xUAS-wt1bDN;cryaa:eCFP)*^{cn14}	This paper	ZDB-ALT-180604-1
Zebrafish: *Tg(GFP-5xUAS-RFP;cryaa:eCFP)* ^{cn15}	This paper	ZDB-ALT-190528-2
Zebrafish: *Tg(mpeg1*:mCherry;*cryaa*:mCherry)^{cn16}	This paper	ZDB-ALT-190528-3
Zebrafish: *wt1b*$^{\Delta 5/\Delta 5}$	This paper	N/A
Oligonucleotides		
sgRNA used to generate *wt1b*$^{\Delta 5/\Delta 5}$ mutants: 5′-GTCGACGGAATTCCCAGTTACGG-3′	This paper	N/A
Please see Table S3 for primer sequences used in this study	N/A	N/A
Recombinant DNA		
p5E-*mpeg1.1* promoter	Ellett et al., 2011	N/A
pME-*mCherry*	Gift from Nathan Lawson lab	N/A
p3E-*polyA*	Villefranc et al., 2007	N/A
βGI-eGFP:E1b-5xUAS-E1b:RFP-βGI	Gift from the Reinhard W. Köster lab	N/A
pDestTol2pA2AC	Kwan et al., 2007	N/A
Software and Algorithms		
Fiji/ImageJ	NIH	RRID:SCR_002285
GraphPad Prism 7	GraphPad Software	N/A
Imaris 8.4.1	Bitplane	N/A
FlowJo-X	FlowJo	N/A
REST	Pfaffl, 2001; Pfaffl et al., 2002	N/A
Zen	Zeiss	N/A
Other		
Dako Fluorescence Mounting Medium	Dako	Cat#S3023
35 mm Dish, No. 0 Coverslip, 20 mm Glass Diameter, Uncoated	MatTek	Cat#P35G-0-20-C
Avidin/Biotin Blocking Kit	Vector Laboratories	Cat#SP-2001
Certified Low Melt Agarose	Bio-Rad	Cat#9012-36-6

LEAD CONTACT AND MATERIALS AVAILABILITY

Further information and requests for resources and reagents should be directed to and will be fulfilled by the Lead Contact, Nadia Mercader (nadia.mercader@ana.unibe.ch).

EXPERIMENTAL MODEL AND SUBJECT DETAILS

Zebrafish

Experiments were conducted with zebrafish embryos and adults aged 4–15 months, raised at maximal 5 fish/l and maintained under the same conditions: 28°C, 650-700 μs/cm, pH 7.5, the lighting conditions were 14:10 hours (light: dark) and 10% of water exchange a day. Feeding schedule was: three times per day, once artemia (Ocean Nutrition) and twice dry food (ZM-000, Gemma Micron 150 and 300 for larvae, juveniles and adults stages, respectively). Approximately equal sex ratios were used for experiments. As controls, siblings or same-staged animals were used. Experiments were approved by the Community of Madrid "Dirección General de Medio Ambiente" in Spain, the Landesamt für Verbraucherschutz Thüringen, Germany and the "Amt für Landwirtschaft und Natur" from the Canton of Bern, Switzerland. All animal procedures conformed to EU Directive 86/609/EEC and Recommendation 2007/526/EC

regarding the protection of animals used for experimental and other scientific purposes, enforced in Spanish law under Real Decreto 1201/2005. Experiments in Switzerland were conducted under the license BE95/15 and BE64/18. Published strains used in this study include: wild-type AB, *Tg*(*wt1b:eGFP*)^{li1Tg} (Perner et al., 2007), *Tg*(*mpeg1:Gal4*)^{gl24Tg} (Ellett et al., 2011), the newly generated *Tg*(*mpeg1*:mCherry;*cryaa*:mCherry)^{cn16}, *Tg*(*GFP-5xUAS-wt1bDN;cryaa:eCFP*)^{cn14}, *Tg*(*GFP-5xUAS-RFP;cryaa:eCFP*)^{cn15} and *wt1b*$^{\Delta5/\Delta5}$. Transgene sequences are available upon request.

METHOD DETAILS

Construction of mpeg1:mCherry Zebrafish

To generate the *mpeg1:mCherry* transgenic line, the following DNA fragments were assembled using Gateway cloning (Kwan et al., 2007): p5E *mpeg1* promoter element containing a 1.8 kb region upstream of the ATG of the *mpeg1.1* gene (Ellett et al., 2011), pME – mCherry and the p3E-polyA fragment from Villefranc et al. (2007). The entire construct was flanked with Tol2 sites to facilitate transgenesis. The plasmid was injected into one-cell-stage zebrafish embryos and those with strong and broad mCherry expression pattern in macrophages were selected and grown to adulthood. Once reaching an appropriate age, individual fish were crossed with the wild-type AB line to identify suitable founders and establish a stable line, named *Tg(mpeg1:mCherry; cryaa:mCherry)*^{cn16}.

Construction of eGFP:UAS:RFP and eGFP:UAS:wt1bDN Zebrafish

To generate the e*GFP:5xUAS:RFP* line, a fragment containing the *β-globin* intron-GFP:E1b-5xUAS-E1b:RFP-β-globin intron was digested with SnaBI and KpnI from a plasmid (gift from the Reinhard W. Köster lab) and cloned into the *pDestTol2pA2AC* vector (Kwan et al., 2007). A fragment containing *cryaa:eCFP* was assembled downstream of the *RFP* plasmid in the aforementioned plasmid by Gibson cloning. The final entire construct was flanked with *Tol2* sites to facilitate transgenesis. In this line, tissue specific expression of *Gal4* drives the bidirectional transactivation of the UAS leading to the expression of both e*GFP* and *RFP*. The full name of this line is Tg(*βGI-eGFP:5xUAS:RFP-βGI; cryaa:eCFP*)^{cn15}.

To generate the e*GFP:5xUAS:wt1bDN* transgenic line, the *RFP-βGI-cryaa:eCFP* fragment was excised from the aforementioned plasmid containing *βGI-eGFP:5xUAS:RFP-βGI* flanked by *Tol2 sites*. This vector was then assembled by Gibson cloning with: (1) a fragment with a truncated version of zebrafish *wt1b* encoding the first 264 amino acids, (2) a *β-globin intron-polyA* fragment amplified from the aforementioned plasmid *βGI-eGFP:5xUAS:RFP-βGI*, (3) a fragment containing the *cryaa:eCFP* to drive expression of *eCFP* in the crystalline. The entire construct was flanked with *Tol2* sites to facilitate transgenesis. In this line, tissue specific expression of Gal4 drives the bidirectional transactivation of the UAS, leading to the expression of both e*GFP* and *wt1bDN*. The full name of this line is *Tg*(*βGI-eGFP:5xUAS:RFP-βGI; cryaa:eCFP*)^{cn14}.

Generation of wt1b Mutant (wt1b$^{\Delta5/\Delta5}$) Zebrafish

The *wt1b* mutant line was generated by CRISPR/Cas9-mediated genomic engineering. Fertilized wild-type AB zebrafish oocytes were injected with a solution containing the single guide sgRNA (15 ng/μl), *cas9* mRNA (150 ng/μl) and phenol red. From several *wt1b* mutant alleles that were identified a line was generated (following *WTABJxTü* outcross) harboring a 5 base pair deletion within exon 2 of *wt1b* and named *wt1b*$^{\Delta5}$ (Figure S3E). The specific allele is predicted to cause a premature stop codon (Figure S3F). To screen *wt1b*$^{\Delta5/\Delta5}$ mutant animals, a PCR and subsequent digestion of the PCR amplicon with the restriction enzyme BsrI was performed. In *wt1b*$^{\Delta5/\Delta5}$ mutant animals, a unique undigested 480 bp DNA band can be identified. Primers used for genotyping are described in Table S3.

Zebrafish Cardiac Cryoinjuries

Cardiac ventricular cryoinjury experiments were conducted using adult zebrafish as described (González-Rosa and Mercader, 2012). Briefly, adult fish were anesthetized and their pericardial cavity opened to expose the heart. A copper filament cooled in liquid nitrogen was placed on the ventricular surface of the heart until thawing. After surgery, animals were revived by gently directing water to their gills using a plastic Pasteur pipette.

Zebrafish Caudal Fin Amputations

Larval and adult caudal fins amputations were performed using a scalpel. For larvae, caudal fin amputations were performed at 3.5 or 4.5 dpf including the very distal part of the notochord. For adults, amputations were performed only to half of the caudal fin.

Zebrafish Histological Analysis and Imaging

Adult zebrafish were euthanized by immersion in 0.16% tricaine and hearts dissected and processed as described in González-Rosa and Mercader (2012). Samples were fixed overnight at 4°C in 2% PFA and included in paraffin or gelatin following conventional histological procedures. Immunofluorescence of paraffin- or gelatin-embedded 7 μm sections or whole mount zebrafish embryos was performed as described in González-Rosa et al. (2011). Briefly, samples were permeabilized with 0.5% Triton X-100 in PBS, blocked in histoblock (5% BSA, 5% goat serum, 20mM $MgCl_2$) for 2 hours at room temperature, and incubated with primary antibodies in PBS containing 5% BSA overnight at 4°C. Samples were incubated with secondary antibodies at room temperature for 2 hours and incubated with DAPI for 10 minutes. Primary antibodies used were: chicken anti-GFP (Aves, 1:250), rat anti-mCherry

(Invitrogen, 1:250), mouse anti-DsRed (Takara, 1:250), rabbit anti-L-plastin (a kind gift from Paul Martin; 1:500), anti-Myosin Heavy Chain (DSHB Iowa Hybridoma Bank (MF20 for paraffin sections or F59 for gelatin sections, 1:20), mouse anti-BrdU (BD PharMingen; 1:250), rabbit anti-WT1 (a kind gift from Elizabeth Patton; 1:1000) (Lopez-Baez et al., 2018). Secondary antibodies were Alexa Fluor 488, 568, 647 (Life Technologies, 1:250) and biotin anti-rabbit (Jackson Immuno Research, 1:250) or biotin anti-rat (Jackson Immuno Research, 1:250) followed by incubation with Cy3 or Cy5 streptavidin conjugate (Molecular Probes, 1:250). Nuclei were counter-stained with DAPI and slides were mounted in Dako Fluorescence Mounting Medium.

To detect *wt1b*, *mafbb, mmp14a* and *mCherry* transcripts, RNAScope (Advanced Cell Diagnostics) was performed following the manufacturer's instructions for PFA-fixed paraffin-embedded samples with standard tissue pretreatment and Fluorescent Multiplex Assay detection kit. Following transcript detection, an anti-GFP immunofluorescence was performed on the same slides.

A Zeiss LSM 880 or Leica SP8 confocal microscopes were used to image immunostained sections.

Acid fuchsin-orange G (AFOG) stain was used to detect fibrotic tissue. Muscle, fibrin/cell debris and collagen were stained brown-orange, red and blue, respectively.

FACS and Flow Cytometry

Hearts collected in ice-cold PBS were digested at room temperature in 0.5% trypsin and repeatedly passed through a micropipette tip to obtain a single cell suspension. Digestion was stopped by adding ice-cold PBS, 10% fetal bovine serum (FBS), and cells were pelleted by centrifugation (200 x g, 10 min, 4°C) and resuspended in 10% FBS in PBS. Dead cells were excluded by staining with 1 μg/ml DAPI (Sigma). Cells were analyzed for forward scatter, side scatter and eGFP and mCherry fluorescence on an Aria Canto 3L HTS FAC (Beckton Dickinson). Percentages of mCherry$^+$ and mCherry$^+$;eGFP$^+$ cells were determined by analyzing 100,000 cells per sample.

WKM was isolated following dissection of adult kidney tissue, which was pressed through a 40 μm cell strainer. Cells were pelleted by centrifugation (300 g, 5mins, 4°C) and resuspended in PBS and analyzed on a BD FACS Aria Illu device (Beckton Dickinson). Gating for transgenic cells was controlled prior to analysis with non-transgenic control samples. For all samples, debris, doublets and dead cells (SYTOX Blue+,ThermoFisher Scientific) were removed from analysis.

WKM experiments were performed with a sequential application of two interim analyses prior to final statistical calculations (Neumann et al., 2017). Significance levels were applied with interim α-values of 0.001 to avoid type I errors and a final α- value of 0.05. Three replicates with total n numbers *wt1b*$^{+/+}$ = 15, *wt1b*$^{+/\Delta5}$ = 15, *wt1b*$^{\Delta5/\Delta5}$ = 14 were performed. WKM experiments were analyzed using FlowJo-X and plots were generated using R (ggplot2 package).

Cytology

Kidney- and cardiac-derived *wt1b*:eGFP$^+$;*mpeg1*:mCherry$^+$ and *mpeg1*:mCherry$^+$ cells were isolated as described in "FACS and Flow Cytometry" section, separated by FACS and concentrated by cytocentrifugation at 250 x g for 5 min onto glass slides using a Shandon Cytospin 4 (Thermo Fisher Scientific). Slides were fixed and stained with May-Grünwald Giemsa protocol as described in Stachura et al. (2009). Briefly, samples were fixed in methanol for 15 minutes, May- Grünwald for 20 minutes, washed with dd$H_2$0 followed by Giemsa staining for 10 minutes, washed with dd$H_2$0, briefly dried and mounted with DPX.

RT-qPCR on Heart Samples

Hearts from *Tg(wt1b:eGFP;mpeg1:mCherry)* zebrafish were cryoinjured and at 4 dpi mCherry$^+$ and eGFP$^+$;mCherry$^+$ cells were FACS purified. RNA was extracted and a total of 1 μg of RNA was reverse-transcribed into cDNA with random hexamers. Quantitative PCR (qRT-PCR) was performed on a 7500 Fast ABI System (Invitrogen Life Technologies). PCR cycles proceeded as follows: initial denaturation for 30 s at 95°C, followed by 40 cycles at 95°C for 5 s and 60°C for 30 s. Melting curve analysis was performed in SYBR green reactions to show PCR product specificity. To calculate the relative index of gene expression, we employed the $2^{-\Delta Ct}$ method, where *ef1*α gene served as the internal control. Primers used are described in Table S3.

RT-qPCR for wt1a and wt1b in Zebrafish Larvae

Total RNA was isolated from larvae at 5 dpf using trizol according to the manufacturer's protocol. 10 samples containing 10 *wt1b*$^{\Delta5/\Delta5}$ or *wt1b*$^{\Delta5/\Delta5}$ larvae each were collected per genotype. RNA was reverse transcribed with iScript cDNA synthesis kit (Bio-Rad) and qRT-PCR was carried out in triplicates for each sample using SYBR GreenER (Thermo Fisher Scientific) on the CFX384 Real-Time System (Bio-Rad). PCR efficiencies and relative expression were calculated, and significances determined by using pairwise reallocation randomization test (using REST) as previously described (Pfaffl, 2001; Pfaffl et al., 2002). For normalization we used *ef1*α. Primers used are described in Table S3.

RNaseq Analysis

Hearts from *Tg(wt1b:eGFP; mpeg1:mCherry)* zebrafish were cryoinjured and eGFP$^-$;mCherry$^+$ and eGFP$^+$;mCherry$^+$ cells were FACS purified at 4 dpi. RNA was extracted from 4 pools of eGFP$^-$/mCherry$^+$ and of eGFP$^+$;mCherry$^+$. One ng of RNA was used to generate barcoded RNA-seq libraries using the Ovation Single Cell RNA-Seq System (NuGEN) with two rounds of library amplification. The size of the libraries was calculated using the Agilent 2100 Bioanalyzer. Library concentration was determined using the Qubit fluorometer (ThermoFisher Scientific). Libraries were sequenced on a HiSeq2500 (Illumina) to generate 60 base single reads. FastQ files for each

sample were obtained using CASAVA v1.8 software (Illumina). Four biological replicates consisting of five pooled hearts were used per sample.

Sequencing adaptor contaminations were removed from reads using cutadapt 1.7.1 software (Martin, 2011) and the resulting reads were mapped and quantified on the zebrafish genome (Zv11, release 94) using RSEM v1.2.20 (Li and Dewey, 2011). Only genes with at least 1 count per million in at least 4 samples were considered for statistical analysis. Data were then normalized and differential expression tested using the Bioconductor package limma (Robinson et al., 2010). We considered as differentially expressed those genes with a Benjamini-Hochberg adjusted pvalue < 0.05 and abs(Log_2FC > 1). Raw data has been deposited in the GEO Database with the reference GEO: GSE115381.

GO Biological Processes enrichment analysis

We used the R language Clusterprofile package (Yu et al., 2012). Differentially expressed genes (Benjamini-Hochberg adjusted pvalue < 0.05) were used with *enrichDavid* function with the parameters (pvalueCutoff = 0.01 annotation = 'GOTERM_BP_ALL'). Further $zscore = (up - down/\sqrt{genes})$column was included using R for circular plotting with GOplot package and GOChord function (Walter et al., 2015). The workflow can be visualized using Docker and has been deposited in https://doi.org/10.17632/v2fyxb8rjy.1.

Macrophage Migration Assay

Larvae were transferred to E3 medium containing 0.2 mg/ml tricaine and 0.0033% phenyl-thiourea and immobilized in 1% low melting agarose in a 35 mm Petri dish with a glass cover. The caudal fin was transected with a sterile scalpel at 3.5 dpf or 4.5 dpf in *Tg(wt1b:eGFP;mpeg1:mCherry)* or the *UAS*-driven lines, respectively. Amputated larval caudal fins were imaged from 0.5 to 12 hpa using a Zeiss LSM 880 inverted confocal microscope with a 20x air objective. A z stack of 100 μm was acquired every 5 min for *Tg(wt1b:eGFP;mpeg1:mCherry)* line and every 10 min for the *Tg(mpeg1:Gal4;eGFP-UAS-RFP)* and *Tg(mpeg1:Gal4;eGFP-UAS-wt1bDN)* lines. The 4D files generated from time-lapse acquisitions were processed using Zen software and compressed into maximum intensity projections. Brightness, contrast, and color levels were adjusted for maximal visibility and drift correction was applied. Migration speed of macrophages was quantified using the points and statistic function in Imaris. The average of macrophage subpopulation mean migration speed was calculated for each embryo.

Macrophage Intensity Analysis

Tg(wt1b:eGFP;mpeg1:mCherry) 3.5 dpf larvae were subjected to caudal fin amputation and imaged from 0 to 34 hpa using a Zeiss LSM 880 inverted confocal microscope with a 20x air objective. A z stack of 100 μm was acquired every 5 min using 2x1 tile scan, which were then stitched together using Zen software. In FIJI, a maximum intensity projection followed by a 2 pixel (Px) mean filter was applied to the time-lapse data to increase the homogeneity within individual cells. The ImageJ MtrackJ tool was used to analyze the migration of macrophages. For cell tracking the intensity signal was measured by applying the local cursor snapping function to detect the Px with the maximal fluorescence intensity within a cell. Starting from the last time point, double positive *wt1b*:GFP^+;*mpeg1*:$mCherry^+$ cells were tracked back until their first appearance. Subsequently, the tracked XY coordinates and the GFP fluorescence intensity over time were exported. To correct for growth and obtain a reference location the amputation site was tracked. The analysis was performed in MATLAB R2017a.

Each cell was categorized whether it is migrating positive for *wt1b*:GFP or is upregulating *wt1b*:GFP expression while migrating toward the injury. Two criteria to categorize for migration or activation were defined: First criterion for migration, once during its first five time-points (25 min), after appearance, the cell has to pass 33% of its own maximal GFP intensity. Second criterion, the cell has to be in the 25% most anterior tracked distance to the injury site during one of the first five time-points after appearance. The percentage of migration versus activation in each embryo was calculated and from these the mean percentage was obtained.

Each measured intensity was divided by the maximal measured GFP intensity of the individual embryo to increase comparability. The time-course was divided in 20 intervals (binning of 20 × 5 min). The mean intensities per embryo and mean intensities of all embryos per interval were calculated.

Whole Kidney Marrow Transplantation Assays

A previously published protocol was followed with minor modifications (Li et al., 2015). Briefly, wild-type AB zebrafish were irradiated (23 Gy, 7 min). WKM cells from donor *Tg(wt1b:GFP;mpeg1:mCherry)* adult fish were isolated in ice-cold PBS and repeatedly passed through a micropipette tip to obtain a single cell suspension. Then, cells were pelleted by centrifugation (200 g, 10 min, 4°C) and re-suspended in PBS. Cells were transplanted into irradiated fish by retro-orbital injection and, after two weeks, to allow reconstitution of the hematopoietic stem cell niche, hearts were cryoinjured and collected at 4 dpi.

Adult Caudal Fin Regeneration upon Amputation

Caudal fin amputation was performed to wild-type $wt1b^{+/+}$ or mutant $wt1b^{\Delta 5/\Delta 5}$ adult zebrafish. The 3 most regrown rays were measured per animal and time-point and normalized by the initial amputated fin length.

BrdU Pulse-Chase Experiments during Heart Regeneration

Ventricular cryoinjury was performed to wild-type *wt1b*$^{+/+}$ or mutant *wt1b*$^{\Delta5/\Delta5}$ adult zebrafish. At 6 dpi, animals were injected intraperitoneally with 20 μL of 2.5 mg/ml BrdU in phosphate buffered saline (PBS) and hearts were collected at 7 dpi. To calculate BrdU cardiomyocyte labeling indices, ventricular sections were immunostained with anti-MHC and anti-BrdU, antibodies and nuclei counterstained with 4′6-diamidino-2-phenylindole (DAPI). 3 ventricular sections containing the largest injury areas were imaged per heart. BrdU^{+};MHC^{+} cardiomyocytes were counted manually using ImageJ software in the whole ventricle and then normalized by total ventricular MHC area. The cardiomyocyte proliferation index from individual sections was averaged to establish a proliferation index for each animal.

Macrophage Localization Assessment in Regenerating Hearts

Ventricular cryoinjury was performed to *Tg(wt1b:eGFP;mpeg1:mCherry)* either *wt1b*$^{+/+}$ or *wt1b*$^{\Delta5/\Delta5}$ adult zebrafish and hearts were collected at 7 dpi. *mpeg1:mCherry*$^{+}$ and *wt1b:eGFP*$^{+}$*;mpeg1:mCherry*$^{+}$ macrophages localized in the whole ventricle and those localized in the 100 μm of myocardium surrounding the injury area were manually counted and classified according to their relative position to the cryoinjured area.

Quantification of Fibrotic Tissue in Regenerating Hearts

To quantify the fibrotic area in regenerating hearts at 7 and 28 dpi, images of evenly-spaced AFOG-stained serial sections of the whole heart were scanned. Masks of every ventricular section per slide were manually generated and quantified using ImageJ Threshold Color based on differential staining: muscle (brown/orange); fibrotic area (fibrin (red) and collagen (blue)). To calculate the percentage of ventricular injured area, the total fibrotic area was normalized to the total ventricular area for each heart.

QUANTIFICATION AND STATISTICAL ANALYSIS

Sample sizes were chosen based on previous publications and are indicated in each figure legend. The experiments were not randomized, and the investigators were not blinded to allocation during experiments and outcome assessment. All statistical values are displayed as mean ± standard deviation. Sample sizes, statistical test and P values are indicated in the figures or figure legends. Data normality was determined before using parametric or non-parametric statistical test. All statistical tests were performed using GraphPad Prism 7 software.

DATA AND CODE AVAILABILITY

Raw data has been deposited at Mendeley under the link https://doi.org/10.17632/v2fyxb8rjy.1. RNA-seq raw data has been deposited in the GEO Database with the reference GEO: GSE115381. Zebrafish line information has been deposited at ZFIN.